AD-A035 710 SYSTEMS SCIENCE AND SOFTWARE LA JOLLA CALIF F/G 14/2
REVIEW AND DEVELOPMENT OF GROUND MOTION AND AIRBLAST INSTRUMENT--ETC(U)
JUN 76 P L COLEMAN, E S GAFFNEY, W G GINN DNA001-75-C-0008
UNCLASSIFIED SSS-R-76-2945 DNA-4036F NL

1 OF 2
AD A035710

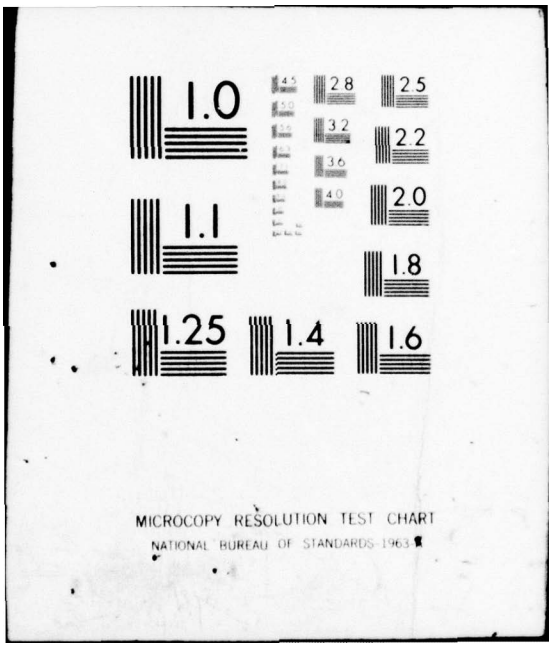
1.0
1.1
1.25
1.4
1.6
1.8
2.0
2.2
2.5
2.8
3.2
3.6
4.0
MICROCOPY RESOLUTION TEST CHART
NATIONAL BUREAU OF STANDARDS-1963-A

DNA 4036F

REVIEW AND DEVELOPMENT OF GROUND MOTION AND AIRBLAST INSTRUMENTATION

Systems, Science and Software
P.O. Box 1620
La Jolla, California 92038

30 June 1976

Final Report for Period 26 August 1975—30 June 1976

CONTRACT No. DNA 001-76-C-0008

APPROVED FOR PUBLIC RELEASE;
DISTRIBUTION UNLIMITED.

THIS WORK SPONSORED BY THE DEFENSE NUCLEAR AGENCY
UNDER RDT&E RMSS CODE B344076462 J11AAXSX35244 H2590D.

Prepared for
Director
DEFENSE NUCLEAR AGENCY
Washington, D. C. 20305

Destroy this report when it is no longer needed. Do not return to sender.

UNCLASSIFIED

SECURITY CLASSIFICATION OF THIS PAGE (When Data Entered)

REPORT DOCUMENTATION PAGE	READ INSTRUCTIONS BEFORE COMPLETING FORM
1. REPORT NUMBER: DNA 4036F	2. GOVT ACCESSION NO. / 3. RECIPIENT'S CATALOG NUMBER
4. TITLE (and Subtitle): REVIEW AND DEVELOPMENT OF GROUND MOTION AND AIRBLAST INSTRUMENTATION.	5. TYPE OF REPORT & PERIOD COVERED: Final Report for Period 26 Aug 75—30 Jun 76
	6. PERFORMING ORG. REPORT NUMBER: SSS-R-76-2945
7. AUTHOR(s): P. L. Coleman, E. S. Gaffney, W. G. Ginn, H. R. Kratz, C. F. Petersen	8. CONTRACT OR GRANT NUMBER(s): DNA 001-76-C-0008
9. PERFORMING ORGANIZATION NAME AND ADDRESS: Systems, Science and Software, P.O. Box 1620, La Jolla, California 92038	10. PROGRAM ELEMENT, PROJECT, TASK AREA & WORK UNIT NUMBERS: Subtask J11AAXSX352-44
11. CONTROLLING OFFICE NAME AND ADDRESS: Director, Defense Nuclear Agency, Washington, D.C. 20305	12. REPORT DATE: 30 June 1976
	13. NUMBER OF PAGES: 106
14. MONITORING AGENCY NAME & ADDRESS (if different from Controlling Office)	15. SECURITY CLASS (of this report): UNCLASSIFIED
	15a. DECLASSIFICATION/DOWNGRADING SCHEDULE

16. DISTRIBUTION STATEMENT (of this Report)

Approved for public release; distribution unlimited.

17. DISTRIBUTION STATEMENT (of the abstract entered in Block 20, if different from Report)

18. SUPPLEMENTARY NOTES

This work sponsored by the Defense Nuclear Agency under RDT&E RMSS Code B344076462 J11AAXSX35244 H2590D.

19. KEY WORDS (Continue on reverse side if necessary and identify by block number)

Stress Gauges
Accelerometers
Quartz
Lithium Niobate
Airblast Instrumentation
Shock Wave Measurements
Hardpan I-2B

20. ABSTRACT (Continue on reverse side if necessary and identify by block number)

The overall objective of this report is to discuss the design and use of instruments for measuring large amplitude ground motion and airblast waves induced by explosions. We consider the environment and possible observing techniques of airblast due to chemical and nuclear explosives. Airblast measurements were made on HARDPAN I-2B. After reviewing the state-of-the-art for ground stress gauges, we provide details

NEXT Page

DD FORM 1 JAN 73 1473 EDITION OF 1 NOV 65 IS OBSOLETE

UNCLASSIFIED

SECURITY CLASSIFICATION OF THIS PAGE (When Data Entered)

388507

20. ABSTRACT (Continued)

of stress instruments using quartz and lithium niobate. We describe potential reductions in the "zero-shift" anomaly that plagues precise accelerometer measurements.

PREFACE

We are indebted to D. R. Grine and J. R. Barthel for discussions concerning airblast measurements and to R. E. Rinehart concerning field calibration ideas. C. S. Brown, R. W. Gilkey, L. R. Prasser and P. B. Ritter contributed greatly to the success of our experimental efforts.

We also appreciate the assistance and advice of our COR, Mr. T. E. Kennedy, of the Defense Nuclear Agency Headquarters.

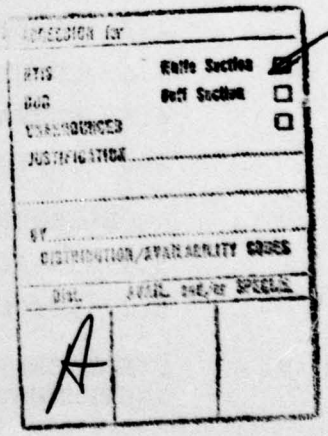

TABLE OF CONTENTS

LIST OF ILLUSTRATIONS

LIST OF ILLUSTRATIONS (cont'd)

LIST OF TABLES

SUMMARY OF CONVERSION FACTORS (U.S. to Metric Units)
AND PREFIXES

To convert from	To	Multiply by
mils	millimeters	0.0254
inches	centimeters	2.54
feet	meters	0.3048
miles	kilometers	1.6093
square inches	square centimeters	6.4516
square feet	square meters	0.0929
cubic inches	cubic centimeters	16.38706
cubic feet	cubic meters	0.0283
gallons(U.S.)	liters	3.785
ounces	grams	28.349
pounds	kilograms	0.454
pounds per square inch, psi	newtons per square centimeter	0.6894757
pounds per cubic inch	kilograms per cubic centimeter	27,679.90
pounds per square foot	newtons per square meter	47.88026
inches per second	centimeters per second	2.54
Fahrenheit degrees	Celsius degrees or Kelvins[a]	5/9
kilotons	terajoules (10^{12} Joules)	4.183

[a]To obtain Celsius (C) temperature readings from Fahrenheit (F) readings, use $C = (5/9)(F - 32)$. To obtain Kelvin (K) readings, use $K = (5/9)(F - 32) + 273.15$.

$1\ Pa = 1\ \frac{N}{m^2}$

$1\ Bar = 10^5\ Pa = 14.5\ psi$

$1\ psi = 6.9\ RPa$

$1\ g$ = Acceleration of gravity = $32\ F/S^2 = 9.8\ m/s^2$

PREFIXES: $G = 10^9$ = giga $M = 10^6$ = mega
$K = 10^3$ = kilo $c = 10^{-2}$ = centi
$\mu = 10^{-6}$ = micro $n = 10^{-9}$ = nano

SECTION I

INTRODUCTION AND SUMMARY

Systems, Science and Software (S^3), under contract to the Defense Nuclear Agency (DNA), has participated during the last three years in a continuing review and development of techniques for measuring transient motion and stress. In two previous reports (Grine and Coleman, 1974, and Coleman, Ginn and Grine, 1975) we considered several types of instrumentation for ground shock studies. In the present report, we emphasize ideas and results concerning airblast observations.

Section II considers a variety of possible methods for monitoring airblast in simulators and cavity shots planned by DNA. These environments present a number of difficulties including entrained, high-speed dust, rapidly varying flow speeds and intense nuclear radiation.

In Section III, we describe our participation in the HARDPAN I-2B event sponsored by the Air Force. S^3 fielded eight airblast transducers. Our data return was good but some significant anomalies occurred at shock arrival.

Section IV presents a review of the currently popular instruments used to measure stress in explosively induced ground motion. We include a number of details on the design and calibration of quartz and lithium niobate stress gauges.

Accelerometers are often used to record details of ground motion. However, when their signals are integrated to give velocity information, the results may contain large errors due to the nonideal performance of the transducer. We discuss this problem in Section V.

Finally, in Section VI we briefly comment on the value of field calibration of ground motion instruments.

SECTION II

AIRBLAST INSTRUMENTATION

2.1 INTRODUCTION

In this section, we discuss the problems of airblast instrumentation. In particular, we summarize the expected environment and the possible ways in which it can be observed. It appears that considerable development will be needed in order to make high quality measurements.

For application in DNA airblast simulators, the unidirectional and non-nuclear nature of the flow somewhat ease the observer's problems. However, there exist two complications. The long duration of the blast, > 50 ms, requires care in the design and fabrication of the instruments. Of greater concern is the dust lofted into and entrained by the shock wave. For a realistic simulation of a nuclear blast, the mass density of the dust should be comparable with that of the gas. The dust may significantly cool the blast wave and contribute to the dynamic pressure. Measuring techniques that are appropriate in clear air may need to be modified for use in a dusty environment. Section 2.2 discusses the instruments usable in airblast simulators.

For application in an underground nuclear cavity shot, the flow direction is not known a priori and all instruments must be radiation hardened or well shielded. In addition, the blast is highly time variable. Because of the spherical geometry and finite size of the source, the air flow behind the shock front (at a fixed observing point) drops from supersonic to subsonic within a millisecond. Most of the available measurement techniques are sensitive to the local Mach number of the flow. Thus to observe, for example, the dynamic pressure, several different techniques must be combined; together they specify Mach number of the flow (not

the Mach number of the shock), ratio of specific heats (γ), and dynamic pressure. Details of these ideas are given in a topical report (Gaffney, Kratz and Barthel, 1976). We summarize that report in Section 2.3.

The majority of the instruments discussed in Sections 2.2 and 2.3 cannot directly determine the flow velocity. In Section 2.4 we analyze a sonic scheme for directly monitoring both the vector flow velocity and the local velocity of sound.

2.2 INSTRUMENTATION FOR AIRBLAST SIMULATOR

Development and testing of high explosively driven nuclear airblast simulators is a continuing DNA program. Simulators such as HEST and FOAMHEST have been developed to simulate the static overpressure loads on shallow buried and surface flush structures. These simulators do not, however, simulate the dynamic pressure resulting from the flow velocity of the air (or air plus dust) behind the shock front. BOSS and DABS are simulators that are designed to simulate the airflow as well as the overpressure. In BOSS the high explosive products are excluded from the simulated airblast, whereas in DABS the trailing portion of the blast wave contains high explosive products. DABS is currently being developed to simulate the flow field from a one-megaton near-surface burst at a range corresponding to a peak static overpressure of approximately 600 psi. For testing structures, it is important that the flow field as well as the overpressure be simulated, because the dynamic pressure in the early portion of the blast wave is considerably greater than the static pressure. In addition, if the simulators are to be of use in the design of the land mobile MX program, it will be important to load the blast wave with dust; the dynamic pressure of the dusty air flow may be more than twice that from air alone.

In this section we consider instrumentation that can measure the flow variables in a simulated airblast. We consider first instrumentation for a blast wave consisting of clean air (or air and HE products) and then we consider changes in the instrumentation and in the interpretation of the data for a dust laden blast wave.

The calculations of Physics International (PI) (Moore, et al., 1975) for the BOSS simulator indicate the characteristics of the flow fields for which instrumentation will be required. These particular calculations are for a design to simulate the airblast from a one-megaton surface burst at a range for which the peak static overpressure is 6.89 MPa (1000 psi). Curves are given for static overpressure versus time, dynamic pressure versus time, and temperature versus time.

In considering airblast instrumentation, the Mach number of the airflow in the blast wave is an important variable. (The reader must distinguish between the Mach number of the flow behind the shock front (i.e., in the blast wave) and the Mach number of the shock front. The Mach number of the flow behind the shock front is relative to the speed of sound in the heated air behind the shock front, whereas the Mach number of the shock front is relative to the speed of sound in the ambient air ahead of the shock front.) The Mach number of the flow behind the shock wave can be determined from the curves for the static and dynamic pressures using the relation

$$p_d = \frac{1}{2} \rho u^2 = \frac{1}{2} \gamma p M^2 \qquad (1)$$

where

p_d = dynamic pressure

ρ = density

u = particle velocity

γ = ratio of specific heats

p = static pressure behind shock front

M = Mach number of flow behind shock front.

Curves of static pressure, dynamic pressure, and Mach number are given in Figures 1, 2 and 3. The calculated temperatures behind the shock front given by Moore, et al. (1975) show that the temperature is greater than 3000°K. At this temperature there is some dissociation and ionization of air and γ is reduced to a value of approximately 1.3, which is the value that was used in calculating M with the above equation. Since M depends on the square root of γ, it is not very sensitive to small variations in γ. The curves of Figures 1, 2 and 3 show that the simulated airblast in BOSS has the following characteristics:

1. a positive phase duration greater than 75 ms
2. the peak static overpressure decreases from 6.89 MPa (1000 psi) to 3.45 MPa (500 psi) in about 13 ms
3. at the front of the blast wave the dynamic pressure is greater than the static pressure by a factor of nearly 3
4. the dynamic pressure decreases more rapidly than the static pressure
5. the flow is initially supersonic (M = 2.1) and decreases to M = 1 in about 30 ms, after which the flow is subsonic.

The duration and rate of change of the airblast suggests that instrumentation with response times of one ms or less will probably be required. It will be necessary that the instrumentation function in both supersonic and subsonic flow, although measurements during the supersonic flow portion of the blast wave probably will be more important.

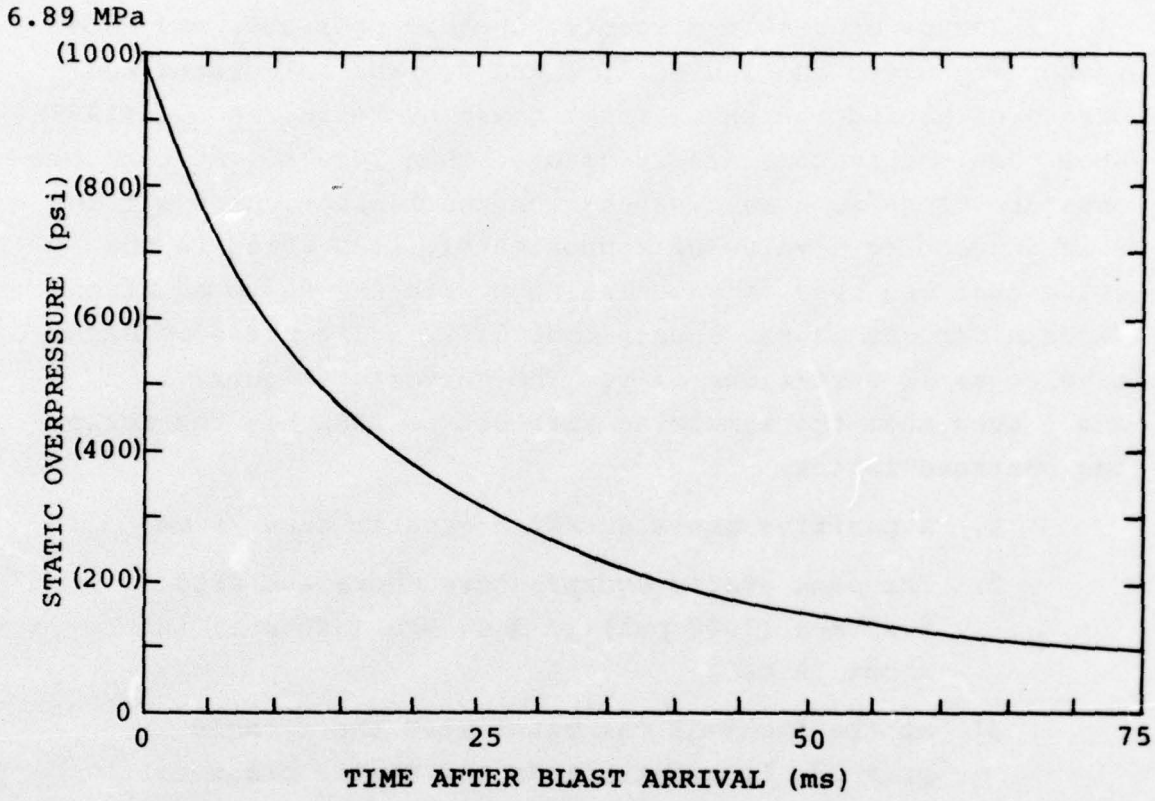

Figure 1. Static overpressure time-history at test station in BOSS.

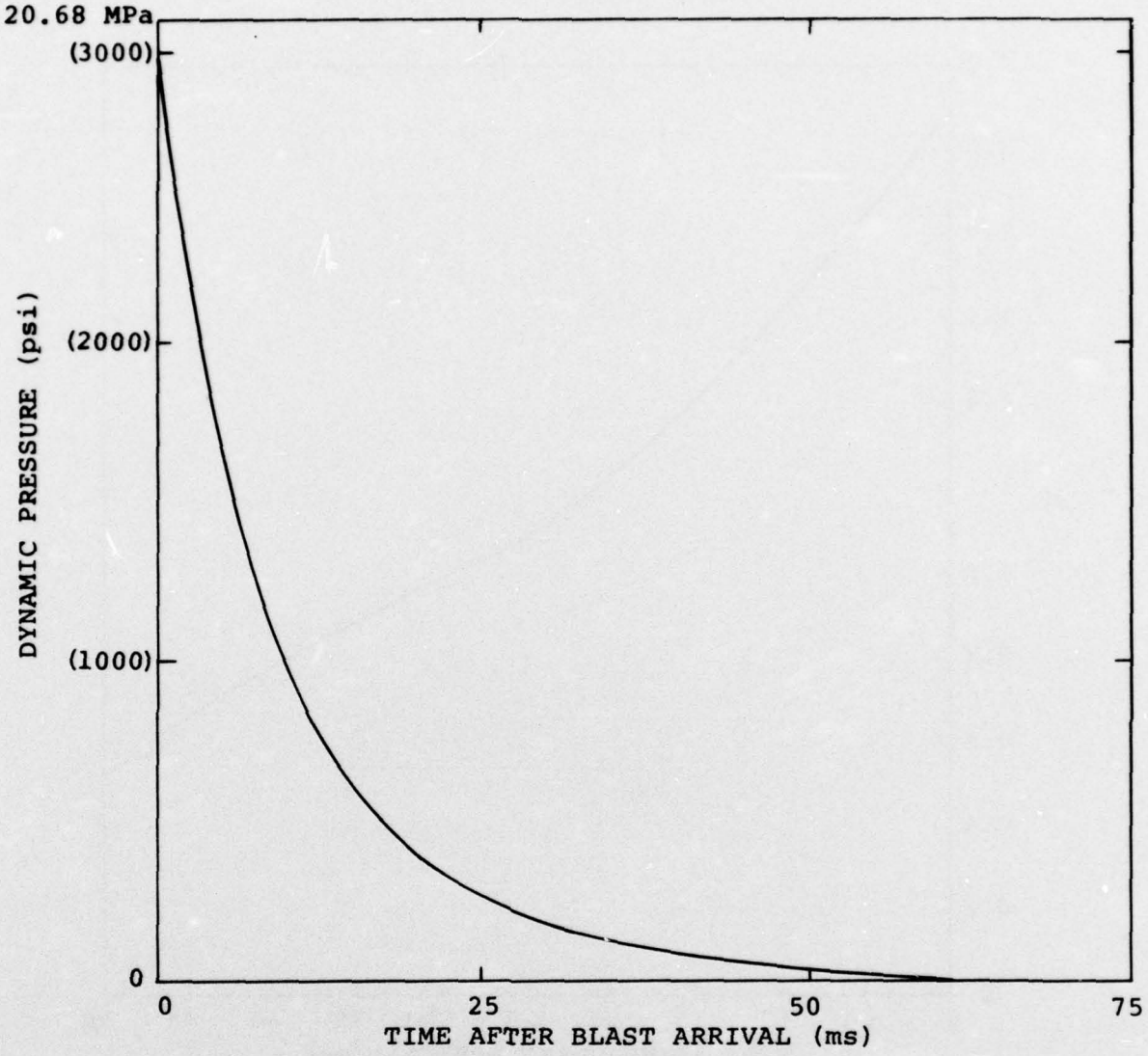

Figure 2. Dynamic pressure time-history at test station in BOSS.

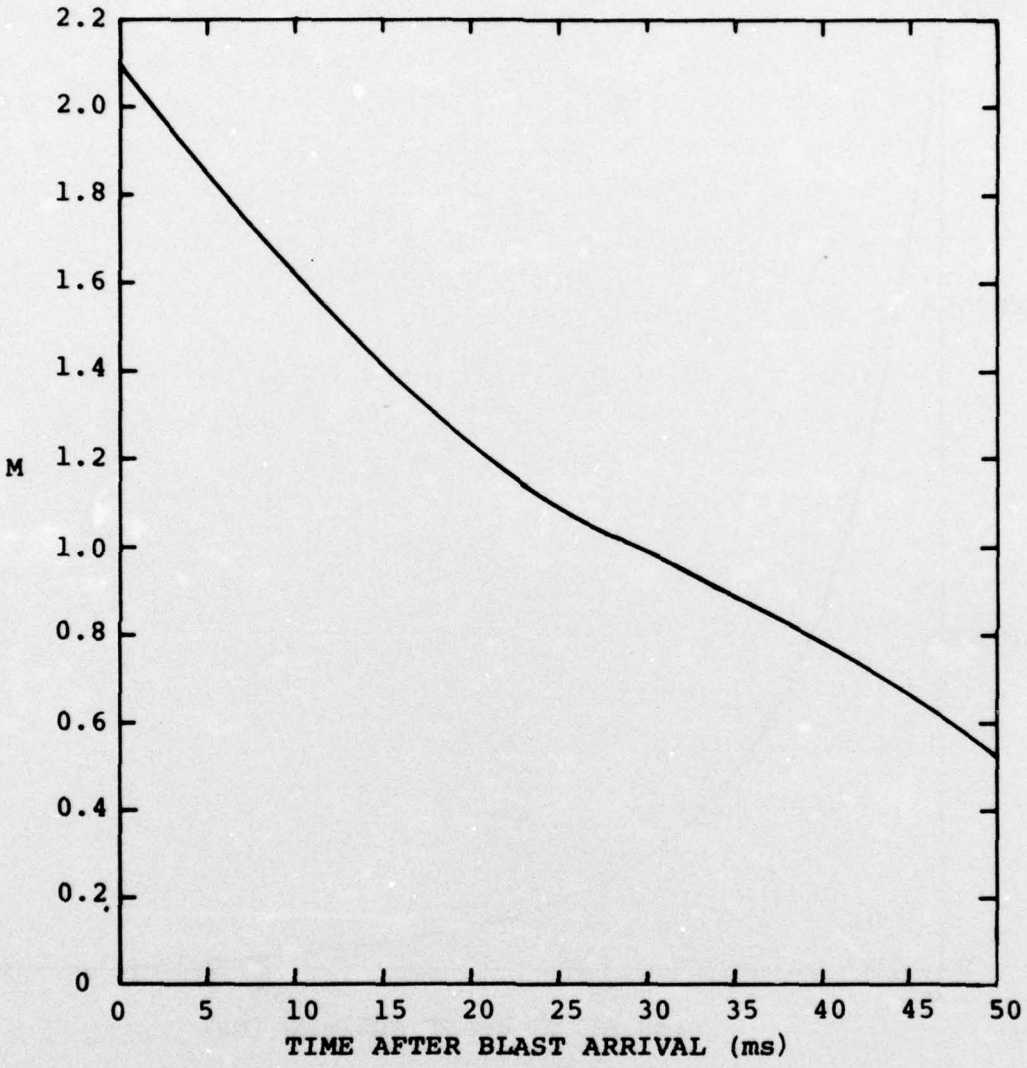

Figure 3. Mach number of flow in blast wave at test station in BOSS.

Since DABS is being designed to operate at a peak overpressure of 4.14 MPa (600 psi) the flow conditions are somewhat different than in BOSS, but the differences are not sufficient to appreciably affect the instrumentation. The flow immediately behind the shock front should have a Mach number of 1.8 and then decrease with time in much the same way as in Figure 3. The temperature at the shock front should be about 1900°C and increase somewhat behind the front. More important considerations affecting instrumentation are likely to be the presence of HE products in the blast wave and the use of dusty atmospheres in the blast simulators.

We assumed that in blast simulators the flow direction is known and does not have to be determined by measurements. Then the flow variables of interest in blast simulators with clean atmospheres are the following:

1. static overpressure
2. stagnation pressure
3. dynamic pressure
4. flow velocity
5. density
6. temperature
7. Mach number
8. sound speed.

In a dusty atmosphere the following additional variables are of interest:

1. dust particle velocity
2. dust density.

At the test station these variables are all functions of time, i.e., they are functions of distance behind the shock front.

In a clean atmosphere below 2000°C, γ is nearly constant and there are equations relating the variables in such a way that if three independent measurements are made, all other variables can be determined. In a dusty atmosphere an additional measurement is required to determine the dust variables. If more than three measurements are made, the redundant measurements are useful as cross-checks on the other measurements. For convenience, we summarize the symbols of the equations in Table 1.

Table 1. Nomenclature

p	= static overpressure in blast wave
p_o	= stagnation pressure
p_d	= dynamic pressure
u	= flow velocity
ρ	= density
ρ_o	= stagnation density
T	= flow temperature (absolute)
T_o	= stagnation temperature (absolute)
M	= Mach number of flow
c_o	= sound speed
γ	= ratio of specific heats
R	= gas constant

The equation relating static pressure and stagnation pressure to Mach number is

$$\frac{p_o}{p} = \left(1 + \frac{\gamma-1}{2} M^2\right)^{\gamma/(\gamma-1)} . \qquad (2)$$

This relation is valid for both subsonic and supersonic flow. However, in supersonic flow there is a bow shock ahead of a stagnation-probe and the pressure measured by the probe is not the true stagnation pressure. In that case the measured pressure is related to the static pressure by

$$\frac{p_m}{p} = \frac{\left(\frac{\gamma+1}{2} M^2\right)^{\gamma/(\gamma-1)}}{\left(\frac{2\gamma}{\gamma+1} M^2 - \frac{\gamma-1}{\gamma+1}\right)^{1/(\gamma-1)}} \qquad (3)$$

where p_m = pressure measured by stagnation probe in supersonic flow. If Equations (2) and (3) are used to determine M from pressure measurements, whether Equation (2) or Equation (3) applies is determined by the measured value of the pressure ratio $\frac{p_o}{p}$ (or $\frac{p_m}{p}$). If the ratio is less than 1.89 in air (with $\gamma = 1.4$), the flow is subsonic and Equation (2) applies; if the ratio is greater than 1.89, the flow is supersonic and Equation (3) applies.

The dynamic pressure is related to the static pressure and Mach number of the flow by

$$p_d = \frac{1}{2} \rho u^2 = \frac{1}{2} \gamma p M^2 \quad ,$$

the sound speed is related to other variables by

$$c_o^2 = \frac{\gamma p}{\rho} \qquad (4)$$

$$c_o^2 = \gamma R T \qquad (5)$$

$$u = c_o M \quad . \qquad (6)$$

Other useful equations relating flow variables are the following

$$p = \rho RT \tag{7}$$

$$\frac{T_o}{T} = 1 + \frac{\gamma - 1}{2} M^2 \tag{8}$$

$$\frac{\rho_o}{\rho} = \left(1 + \frac{\gamma - 1}{2} M^2\right)^{1/(\gamma - 1)} \tag{9}$$

Equations (1) through (9) are sufficient to determine all the flow variables from three independent measurements if the value of γ is known. In clean air at temperatures less than 2000°C, a value $\gamma = 1.4$ is sufficiently accurate for most measurements in blast simulators. When a portion of the blast wave consists of HE products (as in DABS, for example), a value for γ appropriate to the HE products must be used. Fortunately, however, with the exception of Equation (8), the above equations are not very sensitive to small errors in the value of γ in the range of Mach numbers that apply in blast simulators. Dusty atmospheres are a special problem and the value of γ that applies depends upon the properties of the dust and the time period of interest. This problem is considered in more detail later.

Of the many types of instrumentation that are available for measuring flow variables, several types are considered not suitable for use in blast simulators, especially with dusty atmospheres. Simulators such as DABS are one shot devices that are destroyed in each test and we assume, therefore, that the instrumentation probably will be destroyed also.

Pressure measurements on the surfaces of wedges and cones are useful for determining flow direction, but such measurements are not very sensitive to other flow variables such

as Mach number. Also, their response in a dusty atmosphere is not known. Since the flow direction is assumed to be known in blast simulators, wedge and cone measurements do not appear to be very useful.

Hot-wire anemometers are extensively used to measure the temperature in high speed gas flow (Krovasznay, 1954) and in blast waves at large ranges (Batt, 1975). In the hot-wire anemometer, one measures the rate of cooling of a wire which is heated to a temperature higher than that of the gas in which it is immersed. In DABS the temperature will be in excess of 1900°C, which is higher than the maximum usable temperature of platinum wire (Kovasznay, 1954). Also, in order for the anemometer to have a response time of 1 ms, the diameter of the wire must be about 0.00025 cm (Liepmann, 1957); a wire that small in diameter would not be expected to survive in the flow of a blast simulator. For these reasons, we do not think that hot-wire anemometers are feasible for use in blast simulators. An instrument similar to the hot-wire anemometer is a total temperature thermocouple probe (Behrens, 1971), in which the rate of cooling of a small heated cylinder is measured with a thermocouple. In this instrument the cylinder not only has to be heated to a temperature higher than the gas, but it also has to be large enough to accommodate the thermocouple. In practice, the cylinder cannot be made small enough to give a response time as short as 1 ms.

Optical instruments, such as VISARS, interferometers, and Schlieren systems, are widely used in wind tunnels, gas guns, and shock tubes. These are elaborate and expensive systems that would be difficult to use in large simulators such as DABS and might be destroyed in each test. Furthermore, optical instruments that require traversal of the flow field by a light beam will not be usable in a dusty atmosphere. X-ray absorption techniques have been used to measure density at low pressure in wind tunnels. To obtain a

resolution of one ms in a simulator the size and pressure of DABS would require such an intense x-ray source that this technique is not considered to be a practical one.

After reviewing the many types of instrumentation that have been used for measuring flow variables and considering the harsh environments in blast simulators, we recommend fairly simple and inexpensive instrumentation to measure the following variables:

1. static pressure
2. stagnation pressure
3. dynamic pressure
4. Mach number
5. sound speed.

As discussed above, these five flow variables are more than are required to determine all the variables associated with the blast wave and the measurement of all five will give redundant data. We describe below several methods of measuring these flow variables that will be applicable to blast simulators. These techniques will require some development and proof testing. We consider first the case of a clean atmosphere and then the case of a dusty atmosphere.

Static overpressure can be measured with the more or less standard double wedge arrangement shown in Figure 4. Pressure measurements are made downstream from the wedge, on the surfaces of the section of uniform thickness. In order to minimize the flow disturbance, the wedge should be made as thin as possible, consistent with the aerodynamic force to which it is subjected. If the sides of the straight section are parallel with the flow, there is no net force on the wedge because of symmetry. But if there is a misalignment of as little as one degree, the pressure difference on the surfaces of the wedge would initially be about 1.38 MPa

(200 psi) in BOSS and about 0.83 MPa (120 psi) in DABS. This indicates the importance of accurate alignment with the flow, as well as the forces that the support for the wedge would have to withstand.

In order to make the wedge as thin as possible, gauges similar to the S^3 earth pressure gauge can be built into the straight section as shown in Figure 4. Either quartz or lithium niobate piezoelectric crystals can be used, the charge output for a given pressure from lithium niobate being about 15 times that from quartz. Placing gauges on both sides of the straight section would allow any misalignment with the flow to be detected by the pressure difference on the two sides. If there is a small misalignment, the true static pressure can be determined from the two measurements.

The stagnation pressure can be measured with a commercial pressure gauge (e.g., Kistler of Redmond, Washington or PCB of Buffalo, New York) mounted in the end of a heavy walled steel tube so that the active end of the gauge is flush with and closes the end of the tube. The signal lead from the gauge is run through the hole in the tube. The end of the tube can be either square, hemispherical, or ellipsoidal; for the high Reynolds numbers ($> 10^6$) of the flow in blast simulators, the shape of the probe has no appreciable effect on the pressure measurement (Boyer, 1971). Misalignment with the flow of a few degrees also has little effect on the measured pressure. Misalignment can, however, result in a substantial transverse force on the probe body which must be considered in designing the probe mounting.

The dynamic pressure of the air flow can be determined by measuring the acceleration of a sphere suspended in the flow and using the known drag coefficient (approximately unity) for spheres. The problem in measuring a sphere suspended in the flow of a blast simulator is the large displacement of the sphere; in BOSS, the displacement of a 15 cm

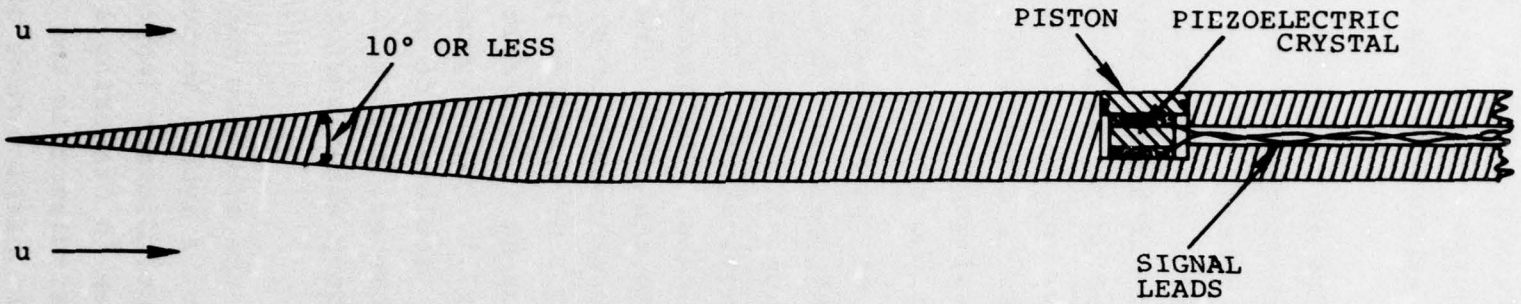

Figure 4. Cross-section of static overpressure gauge. Another piezoelectric measuring element on the other side can be used to measure misalignment with the air flow.

(6-inch) diameter steel sphere would be about 6 meters (20 feet) during the first 50 ms of the blast wave. To alleviate this problem, the same information can be obtained by measuring the force on a sphere supported in the flow as shown in Figure 5. For the Reynolds numbers of flow in blast simulators, the flow behind the sphere is detached from the sphere and the force on the sphere is almost entirely the pressure on the front half. So supporting the sphere as shown in Figure 5 would not appreciably change the force from that on a freely suspended sphere for which the drag coefficient is known. The dynamic pressure of the flow is then given simply by

$$p_d = \frac{f}{\pi r^2 C_D}$$

where

f = force measured by force gauge

r = radius of sphere

C_D = drag coefficient for sphere.

As an example, the initial force on a 10 cm (4-inch) diameter sphere in BOSS would be about 169,000 Newtons (38,000 pounds), decreasing to a low value in about 50 ms. In DABS the initial force would be about 67,000 Newtons (15,000 pounds). Force gauges in this range that would be suitable for these measurements are readily available commercially.

The method proposed to measure Mach number and sound speed is a variation of a technique (Suits, 1935) that has been used previously to measure the temperature in arcs. A diagram of an arrangement for use in a blast wave is given in Figure 6. It consists of two wedges with their straight sides

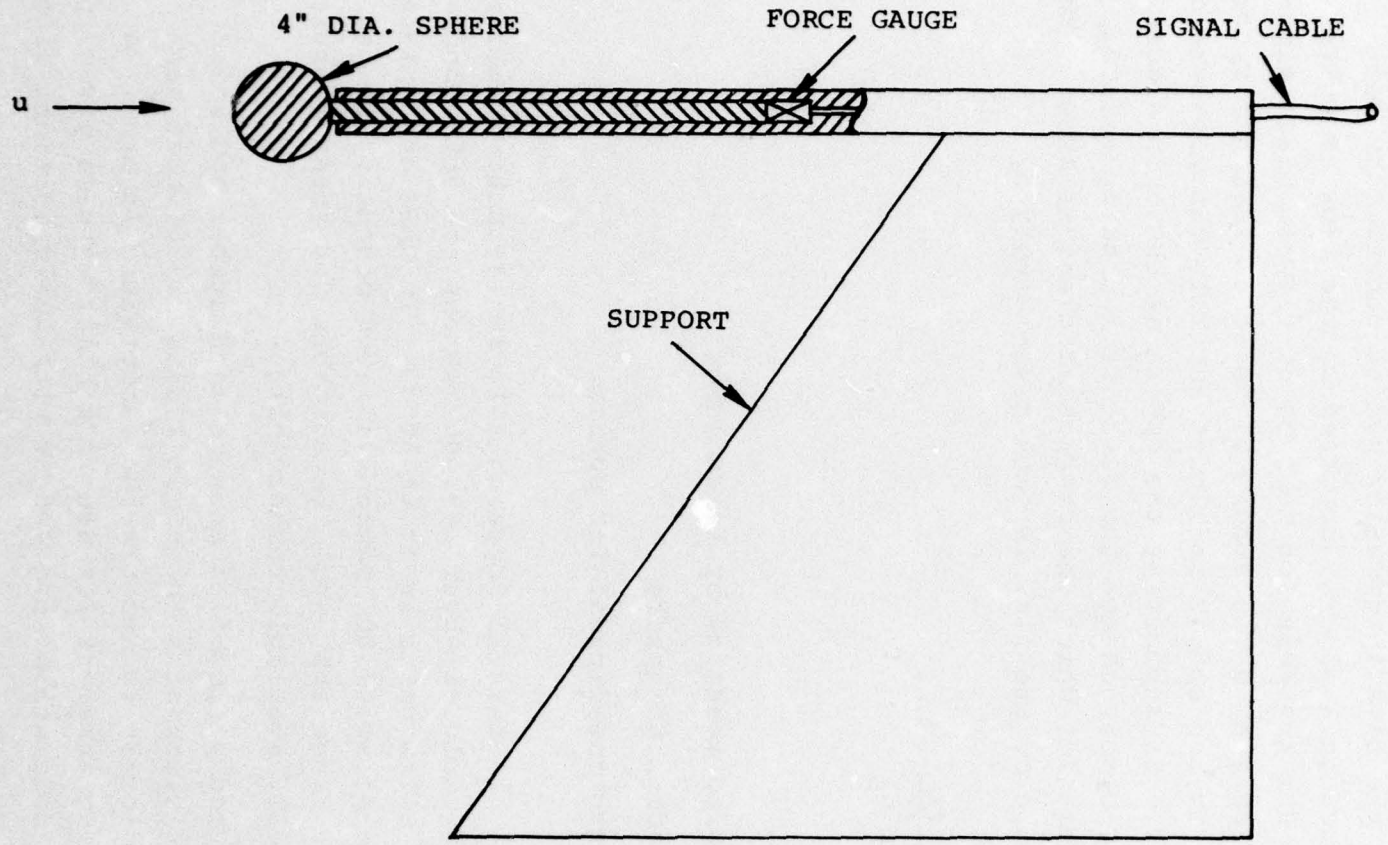

Figure 5. Arrangement for measuring dynamic force by measuring drag on a sphere.

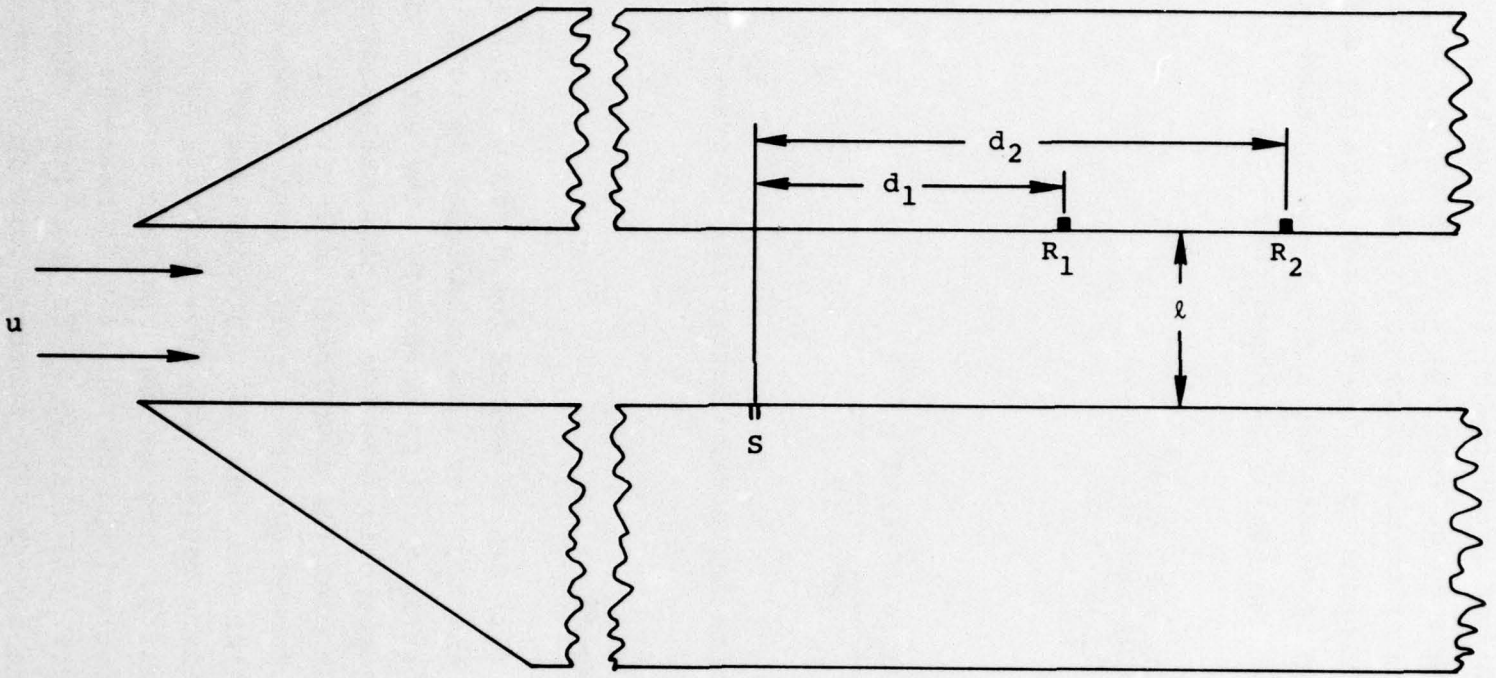

Figure 6. Arrangement for measuring Mach number and sound speed by measuring transit time of a sonic signal between a source and two receivers.

parallel to the flow and separated by about 10 cm as shown. The wedges do not have to be very thick (2 cm or so) in the direction perpendicular to the plane of Figure 6. A source (S) of a sonic disturbance is located on the straight side of one wedge and two receivers (R_1 and R_2) are located on the other wedge. It can easily be shown that

$$t_1 = \frac{d_1 M \pm \left[d_1^2 + \ell^2 \ (1-M^2)\right]^{1/2}}{C_o \ (M^2 - 1)} \tag{10}$$

and

$$t_2 = \frac{d_2 M \pm \left[d_2^2 + \ell^2 \ (1-M^2)\right]^{1/2}}{C_o \ (M^2 - 1)} \tag{11}$$

where t_1 and t_2 = time for sonic disturbance to travel from S to R_1 and R_2

C_o = sound speed.

Equations (10) and (11) can be solved for M and C_o, using measured values of t_1 and t_2. For flow velocities up to M = 2, a restriction is that $d_1 > \sqrt{3}\ell$ in order that the sonic signal arrive at R_1. In supersonic flow two signals are received at R_1 and R_2, the first when the downstream (relative to the flow) edge of the sphere formed by the expanding sonic wave reaches a receiver and a later one when the upstream edge of the sphere arrives at the receiver because the flow velocity is greater than the sound velocity. The second signal is considerably weaker than the first and may be too weak to measure. The minus sign in Equations (10) and (11) apply to the first signal and the plus sign to the second. In subsonic flow only one signal arrives and the minus sign applies.

The sonic source can be a small spark gap that can be fired many times during the passage of the blast wave by using a bank of condensers that are successively discharged. In this way a series of measurements can be made at predetermined intervals during the passage of the blast wave. The receivers can be small piezoelectric crystals embedded in the surface of the wedge so their face (or the electrode on the face of the crystal) is flush with the surface. By having sufficient separation (e.g., 10 cm) between the wedges, effects due to the boundaries layers on the surfaces can be made small. The source and receivers must be located sufficiently far downstream from the front of the wedges so that the effects of the bow shocks which form in front of the wedges in supersonic flow will not affect the measurements. The errors associated with a measurement similar to this one are discussed elsewhere in this report (see Section 2.4). This technique will require considerable development and testing before it will be ready for use in blast simulators.

Flow Measurements in a Dusty Gas. One of the problems in the MX program will be the effect on flow variables, especially on the dynamic pressure, of dust particles that will be popcorned into the air by the thermal pulse, swept up by the blast wave, and remain in suspension to form a dusty gas. Techniques that can be used to measure the flow variables of such a dusty gas depend upon the size of the particles and the characteristic interaction time involved in the measurement. If the particles are small enough they will flow with the gas and change velocity at nearly the same rate as the gas. On the other hand, if the particles are large it may take a considerable time for drag to accelerate the particles up to the velocity of the gas. In the latter case the particles will not follow changes in the velocity or direction of the gas. The size of the particles also determine how closely they follow temperature variations in the gas, i.e., their size

determines whether or not they reach thermal equilibrium with the gas during a measurement. For these reasons, measurements and interpretation of the data in dusty gases depend upon both the particle size and the interaction time involved in making a measurement.

We can determine whether a particular size dust particle is large or small in the above context from estimates of the velocity and thermal relaxation times. The relaxation times are the times required for the velocity and temperature difference between the particle and the gas to be reduced to e^{-1} of their original values. If we assume that the particle drag and heat transfer are described by Stokes flow and a Nusselt number of unity, the velocity and thermal relaxation times are given by (Marble, 1970)

$$\tau_v = \frac{\rho d^2}{18\mu} \tag{12}$$

$$\tau_T = \frac{\rho d^2 c}{12k} \tag{13}$$

where

τ_v and τ_T = velocity and thermal relaxation times

d = particle diameter

ρ = particle density

μ = gas viscosity

k = thermal conductivity of gas

c = specific heat of particle.

Solar furnace experiments (Knasel, 1975) indicate the range in size of dust particles that might be swept up by a blast wave. These experiments indicate a range in diameters from one micron

to 500 microns, with most of the particles being larger in diameter than 40 microns. Using a particle diameter of 40 microns in Equations (12) and (13) gives values for both τ_v and τ_T of about 4 ms.

As a typical flow velocity in a blast simulator we take the velocity at M = 1 and T = 2200°K, giving a flow velocity of about 8×10^4 cm/sec. In most measuring techniques the characteristic interaction distances involved in the measurement are less than 10 cm, giving a characteristic time of about 100 μs. Thus the characteristic interaction time is short compared to the velocity and thermal relaxation times.

It can be shown (Rice, 1976) that γ associated with a dusty gas in which the dust particles are always in thermal equilibrium with the gas is given by

$$\gamma^* = \frac{\gamma + \frac{\alpha_1}{\alpha_2}\frac{c_{v1}}{c_{v2}}}{\left(1 - \alpha_1 \frac{V_1}{V}\right)\left(1 + \frac{\alpha_1}{\alpha_2}\frac{c_{v1}}{c_{v2}}\right)} \tag{14}$$

where

γ^* = ratio of specific heats for dusty gas

γ = ratio of specific heats for clean gas

α_1 = mass fraction of dust

α_2 = mass fraction of gas

c_{v1} and c_{v2} = specific heats at constant volume of dust particles and gas

V_1 = specific volume of the dust particle material, which is assumed to be incompressible

V = net specific volume of dust-gas mixture.

For characteristic times short compared to the thermal relaxation time we can approximate γ^* by taking the limiting case of no energy transfer to the particles, which can be obtained by setting $c_{v1} = 0$ in Equation (14), giving

$$\gamma^* \tilde{=} \frac{\gamma}{\left(1 - \alpha_1 \frac{V_1}{V}\right)} \quad . \tag{15}$$

A typical mass fraction loading of dust is $\alpha_1 = \frac{1}{2}$, with $V_1 = \frac{1}{2}$ cm^3/gm and V = 500 cm^3/gm. Equation (15) then gives $\gamma^* = 1.0005\ \gamma$ (at atmospheric pressure). Even at a pressure of 50 atmospheres we have $\gamma^* = 1.008\ \gamma$. So for measurements in dusty gases of interest, a good approximation is that the γ^* for the dusty gas is the same as γ for the clean gas.

The above considerations have several consequences which relate to measuring flow variables in a dusty gas. Since the dust particles do not respond to velocity changes in the gas during characteristic interaction times for the measurements, and since the γ that applies is that of the clean gas, the sound speed measurement described previously gives the sound speed for clean gas and the Mach number determined by this method is that associated with the flow of the gas. Whether or not the dust particles are flowing at the same velocity as the gas depends upon whether they have been in the flow long enough to have come up to the velocity of the gas, i.e., it depends on how far the particles are from the front of the blast wave. In the front part of the blast wave the dust particles have a velocity small compared to the gas velocity, but further back the velocities are nearly the same.

At the stagnation probe, the dust particles are not deflected by the gas flow but impinge directly on the active area of the pressure gauge and produce a pressure

$$p_p = \rho_p u_p^2$$

where

ρ_p = density of dust, i.e., mass of dust particles per cm^3 of dusty gas

u_p = average velocity of dust particles.

The total pressure measured by the probe is then

$$p_t = p_o + p_p \qquad \text{in subsonic flow} \qquad (16)$$

$$p_t = p_m + p_p \qquad \text{in supersonic flow} \qquad (17)$$

where p_o and p_m are, as defined earlier, the pressures measured by the stagnation probe in clean gas in subsonic and supersonic flow. The static overpressure is not affected by the presence of the dust particles and can be measured in the same way as in clean gas. Using values of M determined in the speed of sound measurements, p_o and p_m can be calculated with Equations (1) and (2). Equations (16) and (17) then give the value of p_p for the dust from the measurements of p_t. Since neither ρ_p nor u_p is measured directly, only $\rho_p u_p^2$ is determined in this way. The variation of $\rho_p u_p^2$ with time will be an indication of the time required for the dust particles to get up to the velocity of the gas, and hence will be an indirect measure [from Equation (12)] of the average size of the dust particles. After the particles are up to the velocity of the gas, ρ_p can be determined, since the velocity of the gas is known from the measurements of M and sound speed. Using a stagnation probe in a dusty gas will probably require that the end of the probe be shaped so that dust does not accumulate and build up to such a thickness that it interferes with the measurement. Using a

conical shape for the probe, with only the active area of the pressure gauge being flat, would prevent such a buildup of dust particles.

Since we have seen that, to a good approximation, γ is not affected by the dust and the measured value of M is the value that applies to the clean gas, the dynamic pressure of the gas can still be determined with Equation (3) from measured values of M and p. Combining the measurements in the manner described above thus gives the flow variables for the clean gas and the dust separately. Whether the force on a sphere suspended in a flow of dusty gas can be used to determine its dynamic pressure depends upon whether the drag coefficient for a sphere in a dusty gas can be determined.

2.3 OBSERVING TECHNIQUES FOR AIRBLAST IN A NUCLEAR CAVITY TEST

At the request of DNA, we considered possible and useful measurements for the HURON KING underground cavity shot. In a recent report, Gaffney, Kratz, and Barthel (1976) discuss potential observations of the airblast, thermal radiation, cratering, ground stress and ejecta size distribution. Perhaps the most interesting and challenging measurements are those of the airblast flow. We summarize below our ideas concerning the very transient cavity airblast.

In the cavity environment, there are three major experimental complications. The flow direction is an unknown to be determined from the data; the instruments must be well-shielded or hardened against the intense γ and neutron radiation generated by the explosion; most of the flow variables change significantly within a fraction of a millisecond after first arrival.

The quantities of most interest are dynamic pressure, $1/2\rho u^2$, the static overpressure, the flow direction and the Mach number, M, of the flow. At a range of 16 meters from a

20 ton explosion, the peak dynamic pressure is estimated to be 8×10^6 Pa (80 bars), the peak static pressure is 3.4×10^6 Pa (34 bars), and the initial Mach number is 1.7. One millisecond after shock arrival, these values have fallen to

$$\frac{1}{2} \rho u^2 \sim 1 \times 10^6 \text{ Pa (10 bars)}$$

$$P_{static} \sim 1.4 \times 10^6 \text{ Pa (14 bars)}$$

and

$$M \sim 1.$$

In general, these quantities cannot be directly observed. Three or four different types of instruments must be used. By correlating their data, we can derive a nearly complete description of the flow field.

Pressure measurements on the downstream surfaces of a slender wedge (Figure 4) do specify the static overpressure. The stagnation pressure at the end of a flat-ended rod gives results analogous to that of a pitot tube. These two measurements combined with Equations (1) through (3) then determine the dynamic pressure and Mach number if the γ of the gas is known or independently observed. In the radiation environment of a cavity test, the basic transducers for the wedge and rod should be bar gauges with the sensing quartz crystals located in the cavity wall.

Tracking the motion of spheres seems to be the most attractive approach for the measurement of the vector flow. For all Mach numbers, the direction of the drag force on the sphere is the direction of the flow. The magnitude of this

force is proportional to the dynamic pressure and the drag coefficient, which in turn is a function of Mach number*:

$$\text{Drag Force} \equiv D = C_d \left(\frac{1}{2} \rho u^2\right) A \tag{18}$$

where

A = cross-sectional area of the sphere, πr^2,

C_D = drag coefficient.

The sphere's motion could be followed optically. However, the opacity of the high-temperature shock front is a significant problem. If the sphere is located at a large enough range, the opacity can be ignored. Then laser velocity interferometers (e.g., an S^3 VISAR) may be used to detect the motion. By using two VISARS at right angles, each at 45 degrees from the direction of the expected motion, we could derive the sphere's vector motion. The VISARS would be fairly expensive.

A better approach is to mount two accelerometers in the sphere. No commercial accelerometers exist with the requisite high output signals and resistance to transient, intense nuclear radiation. Instead, we suggest fabrication of a large area, multi-disc quartz array loaded with a large seismic mass (Figure 7). Coupled with shock mounted Nuvistor cathode followers, this electronic system has been shown (Kratz and Rinehart, 1974) to possess excellent radiation resistance. Because of the transient nature of the cavity airblast, the sphere motion will be only a few centimeters and cable survival should not be a major problem.

---

*In this environment, the Reynolds number exceeds 10^6 and the drag force is insensitive to its exact value.

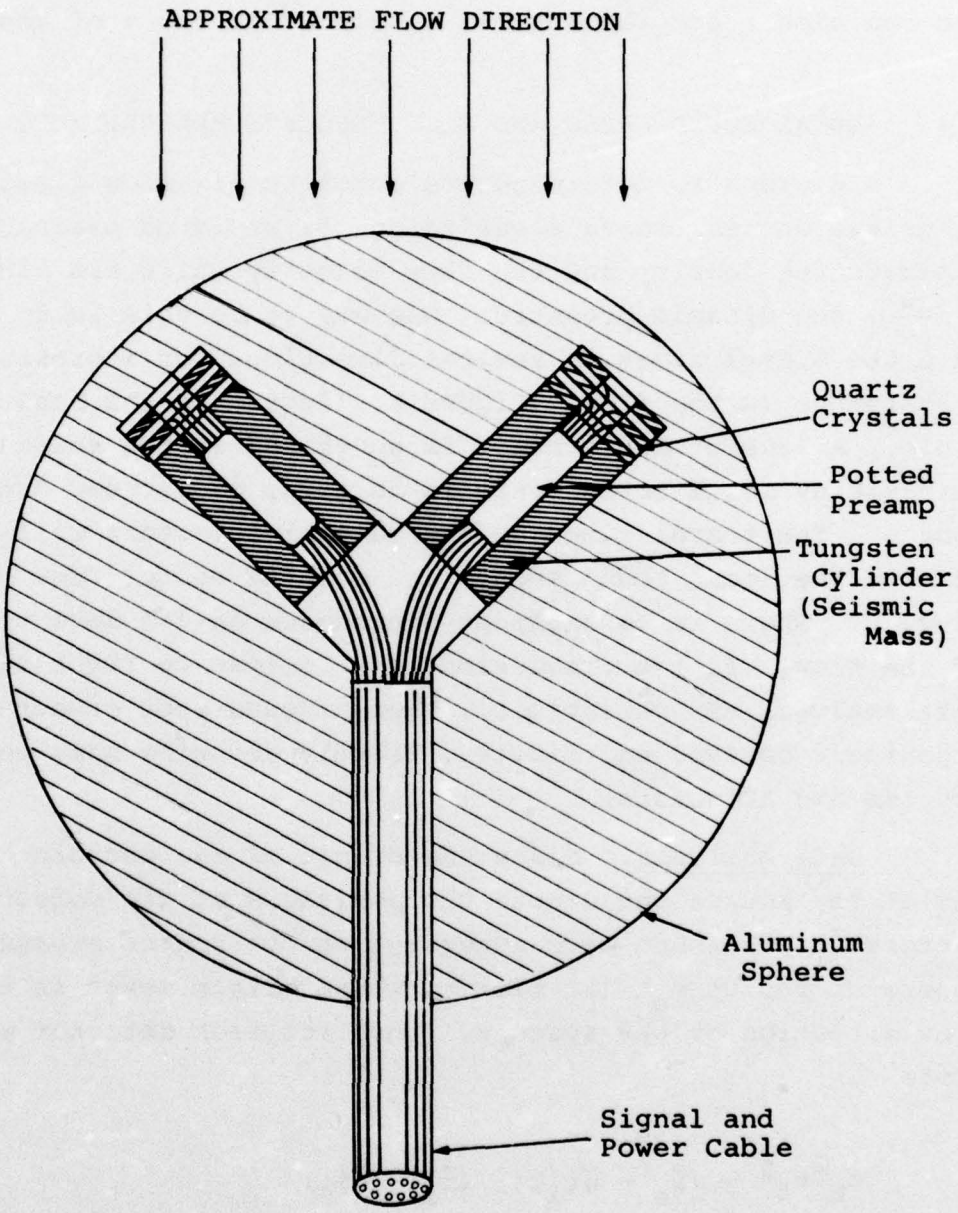

Figure 7. Cross-section of aluminum sphere instrumented with accelerometers to measure flow direction and dynamic pressure.

We emphasize again the value of a variety of instruments. They can provide redundant determinations of the flow variables and can also check the assumed constancy of the γ of the gas.

2.4 LOCAL SOUND SPEED AND FLOW VELOCITY MEASUREMENTS

In order to determine the complete air flow field from a surface or near surface explosion, it would be desirable to separate the density and the flow velocity which are linked as $\frac{\rho u^2}{2}$, the dynamic pressure. One way to do this is to measure the travel times in several directions for a pressure disturbance in the flow. Figure 8 illustrates the basic principle. A "sonic" disturbance is generated at the source and detected by small transducers in an array downstream from the source. The travel times to the several detectors will depend on both the local sound speed, c_o, and the vector flow velocity, $\vec{u}$. There is no explicit dependence on the density, ρ, of the flow. In the discussion that follows we first discuss data analysis and reliability, then discuss some aspects of experiment design, and finally, briefly describe some possible sources and detectors.

Data Analysis. Place the origin of the coordinate system at the source and denote the positions of the detectors by vectors $\vec{r}_i$. A sound wave generated at the source expands as a sphere of radius $c_o t$ (at time t) whose origin moves in the flow direction at the speed u. Thus for each detector we can write

$$c_o^2 t_i^2 = (\vec{r}_i - \vec{u}t_i) \cdot (\vec{r}_i - \vec{u}t_i)$$

$$= |\vec{r}_i|^2 + |\vec{u}|^2 t_i^2 - 2t_i \vec{r}_i \cdot \vec{u} \qquad (19)$$

where t_i is the time interval between generation and reception of the sound signal. There are three unknowns in this relation,

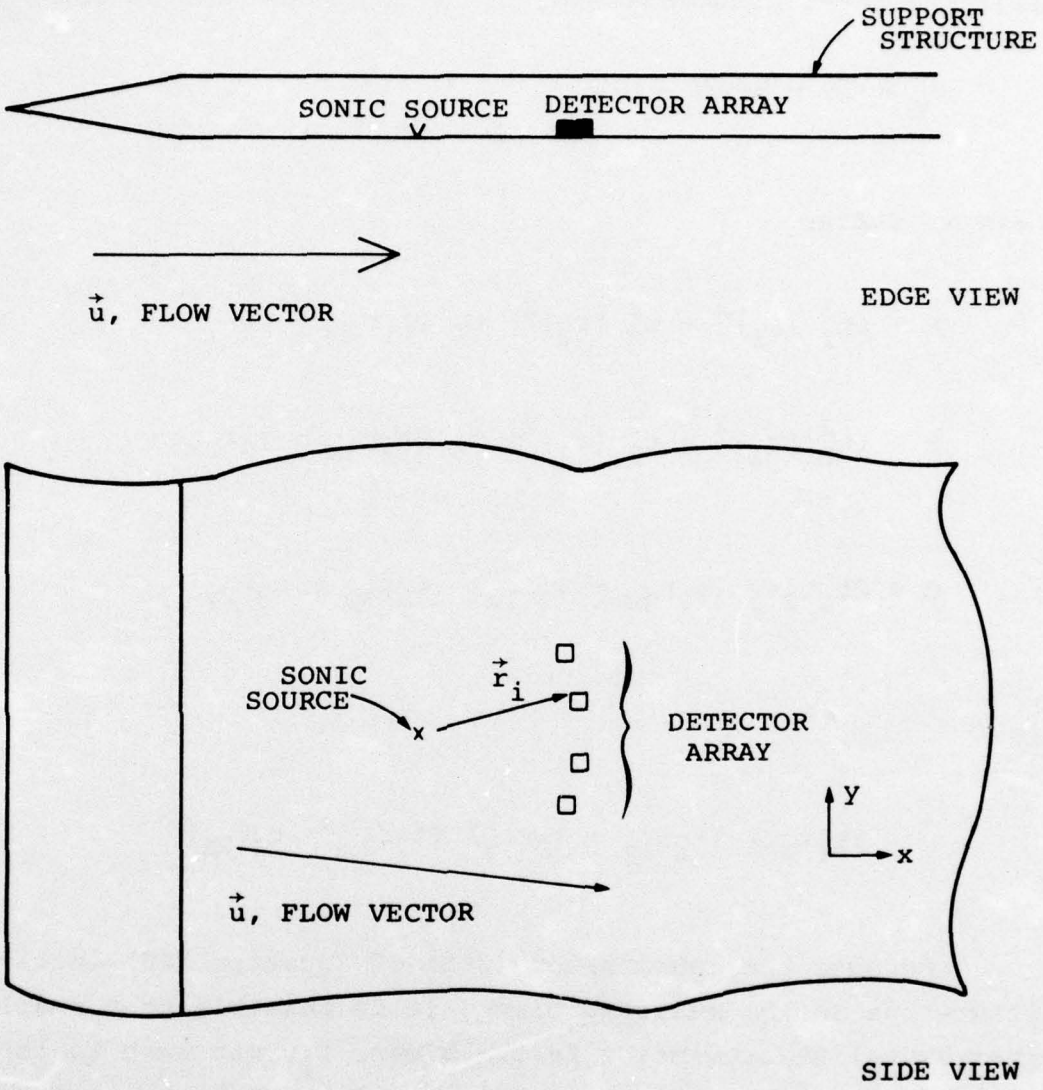

Figure 8. Schematic of instrumentation to measure vector flow velocity and local sound speed. The system is mounted vertically so that the support surface is in the plane of the (2-dimensional) flow.

c_o, u_x and u_y, thus at least three detectors are needed. The resulting three equations can, for example, be solved for u_y*:

$$u_y = (A - B)/(C - D) \tag{20}$$

where we define

$$A \equiv (t_2^2 |r_3|^2 - t_3^2 |r_2|^2)\ t_1\ (t_1 r_{2x} - t_2 r_{1x})$$

$$B \equiv (t_1^2 |r_2|^2 - t_2^2 |r_1|^2)\ t_3\ (t_2 r_{3x} - t_3 r_{2x})$$

$$C \equiv 2t_1 t_2 t_3\ (t_1 r_{2x} - t_2 r_{1x})\ (t_2 r_{3y} - t_3 r_{2y})$$

and

$$D \equiv 2t_1 t_2 t_3\ (t_1 r_{2y} - t_2 r_{1y})\ (t_2 r_{3x} - t_3 r_{2x})$$

Because the denominator (C-D) of Equation (20) involves differences in the measured times, it is possible that small experimental uncertainties in the times, t_i, can lead to large errors in the final results. For example, consider the case that three detectors are equidistant from the source and the vectors $\vec{r}_i$ make angles θ_i of +30°, 0° and -30° with respect to the x axis. If the arrival times observed are

---

*A similar relation holds for u_x: in the numerator of Equation (20) all the x subscripts become y subscripts and the denominator changes sign.

$$\left.\begin{aligned} t_1 &= 100\ \mu s \\ t_2 &= 80\ \mu s \\ t_3 &= 80\ \mu s \end{aligned}\right\} \quad |\vec{r}_i| = 0.1\ m$$

then we find

$$u_x = 543\ m/sec$$

$$u_y = -146\ m/sec$$

and

$$c_o = 722\ m/sec.$$

To investigate the probable errors in these results, we evaluate the logarithmic derivatives of Equation (20):

$$\frac{d\ ln\ u_x}{dlnt_1} = 0.7 \qquad \frac{d\ ln\ u_y}{dlnt_1} = 0.7$$

$$\frac{d\ ln\ u_x}{dlnt_2} = 1.3 \qquad \frac{d\ ln\ u_y}{dlnt_2} = 8.4$$

$$\frac{d\ ln\ u_x}{dlnt_3} = 1.6 \qquad \frac{d\ ln\ u_y}{dlnt_3} = 0.4 \quad .$$

Thus a one ms (1%) uncertainty in the time measurements leads to 2 percent errors in u_x and 8 percent errors in u_y. Note, however, that $u_y/|\vec{u}|$ is small; therefore even fairly large

errors in u_y do not lead to large errors in the direction or magnitude of $\vec{u}$. In addition, the system can readily be expanded to four or more detectors. By correlating the redundant data, the effects of measurement errors will be greatly reduced.

It is obvious that the system's resolution is enhanced for large angular separations between the detectors. But for supersonic flow, a sonic signal will never arrive at a detector if θ is too large; i.e., θ is bounded by

$$\theta < \text{arc sin } \frac{1}{M}$$

for flow along the x axis. For both DABS and HURON KING applications, we are interested in flows up to Mach 2, so θ must be less than 30 degrees.

Experiment Design. The above analysis depends on the existence of a uniform flow field for the duration of the measurements. For simulator applications this will not present any problem since the flow will not vary much over several milliseconds. Hence, the source-detector separations, R, can be as much as 1 m and the analysis will be valid. For HURON KING applications the flow field will be changing by as much as 10 percent per 100 μs in the early part of the flow. Fortunately, both u and c_o are fairly high then so that less than 100 μs would be needed for a signal to get to the detectors at a distance of 0.1 m. Clearly resolution of the flow's details requires that R be as small as possible. On the other hand, 1 μs is probably a reasonable estimate of our time precision for durations near 100 μs, so to minimize the effects of measurement errors, we want R to be as large as possible. A reasonable compromise between these requirements seems to be source-detector separations of about 0.1 m.

In order to achieve our expected precision, we must keep the spacing between the source and the detectors as constant as possible with a minimal perturbation of the flow. One way to do this is to mount the source and the detectors on a rigid plate oriented parallel to the flow as shown in Figure 8. If the front edge of the plate is tapered so that an attached bow shock is formed when $M > 1$, the flow on the flat portion of the plate will be nearly identical to the free field flow. This was discussed in detail in Section 2.2 on static overpressure measurement.

Sources and Detectors. We have not yet considered in detail either sources or detectors for such a system. However, some brief comments are in order. The sonic source should have a large enough amplitude that it will be detectable over the background of the changing flow field. This should be no problem using either an exploding wire or a spark gap to discharge a several microfarad capacitor at several kilovolts. We would prefer a repeating source that can give a signal every quarter- to half-millisecond. Again a spark gap could do this for several milliseconds. Another possibility is a renewable exploding wire, using a mercury filament. Such a device has been studied by Schlumberger (Grine, personal communication) but the details, such as renewal time, are not available to us at present. Small PZT pins would probably serve as suitable detectors.

SECTION III

AIRBLAST MEASUREMENTS ON HARDPAN I-2B

3.1 INTRODUCTION

On 27 August 1975 the HARDPAN I-2B event occurred at Trading Post, Kansas. Systems, Science and Software (S^3) participated by fielding eight airblast gauges. Our objective was to observe the time history of the air overpressure in the test bed. Figure 9 shows the gauge locations and their cable runs. The basic transducers were PCB (Buffalo, New York) 101A02 quartz pressure sensors. These units incorporate a FET buffer amplifier; the effective output impedance is about 100 ohms. Figure 10 summarizes the electrical configuration and Table 2 gives the transducer's specifications.

Each PCB unit was mounted in an aluminum package as shown in Figure 11. This assembly provided protection for the signal connections at the pressure gauge and a rigid termination for the armored cable. The diaphragm of the transducer was mounted flush with the end of the canister cap.

We were aware that these pressure gauges will respond to large heat inputs. Thus we made some effort to reduce their thermal sensitivity. The test bed mounting technique required the gauges be covered by 1/2 inch (1.27 cm) of RTV605 rubber. This coating acted in part as a heat shield. In addition, based on prefielding laboratory tests, a double layer of 2 mil (51 μm) mylar with a 0.5 mil (13 μm) thick coating of aluminum was placed over the active face of the gauge.

Our laboratory thermal tests utilized a commercial photoflash Xenon lamp which had an energy input of 40 joules with a 2 ms duration; the lamp had a BCPS (light output) of 1600 at an ASA rating of 25 for color film. We also used a Sears 275 watt, 110V sun gun to create continuous heat blasts. By holding the Xenon flash about 1/2 inch (1.3 cm) from the

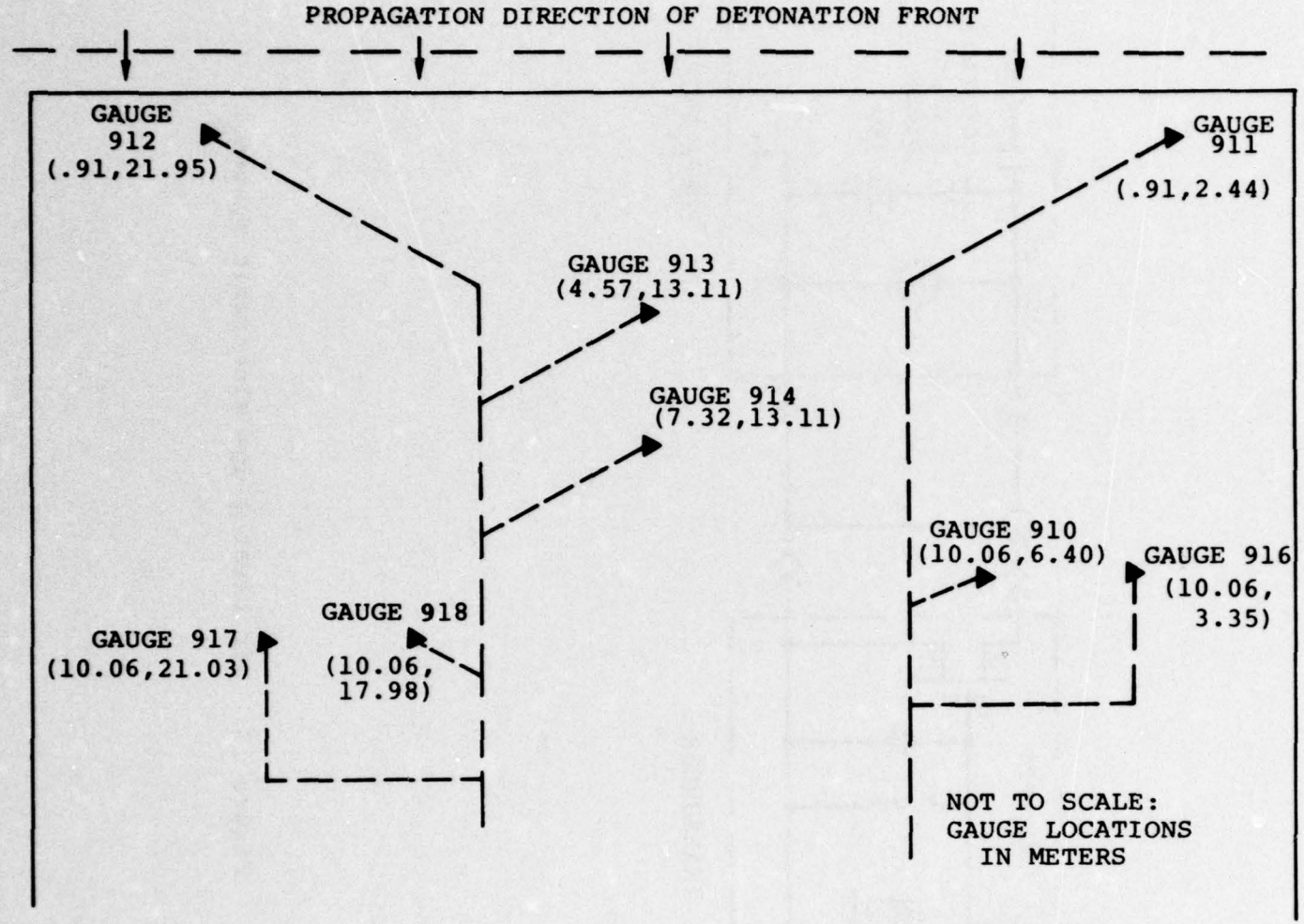

Figure 9. Test bed gauge locations.

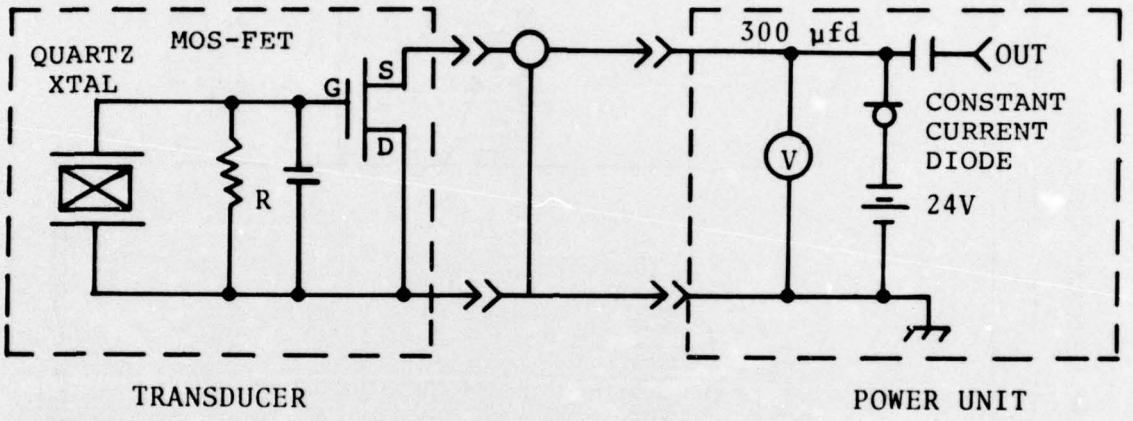

Figure 10. Air blast gauge electronic system.

Table 2. PCB Transducer Specifications

SENSITIVITY (NOM.)	mV/Psi	1 ±.1
RESOLUTION (1)	Psi*	.2
RESONANT FREQUENCY	kHz	400
RISE TIME	µsec	1.0
TIME CONSTANT	Sec	500
LOW FREQUENCY (-5%)	Hz	.001
LINEARITY (2)	%	2
RANGE, F.S. (5V OUT)	Psi	5000
RANGE FOR 10V OUT	Psi	10,000
MAXIMUM PRESSURE	Psi	15,000
OUTPUT IMPEDANCE	Ohms	100
OUTPUT BIAS VOLTAGE	Volts	11
VIBRATION/SHOCK	G, G	2000/20,000
ACCELERATION SENSITIVITY	Psi/G	.002
TEMPERATURE RANGE	°F	-100 to +275
TEMPERATURE SENSITIVITY	%/°F	.03
FLASH TEMP., MAXIMUM	°F	3000
CASE MATERIAL		17-4 PH Stainless Steel
DIAPHRAGM MATERIAL		Invar

(1) 200 uV pk-pk broadband electrical noise.

(2) % F.S., any calibrated range, zero based best straight line.

*1 Psi = 6.9×10^3 Pascal

1 Bar = 10^5 Pascal = 14.5 Psi

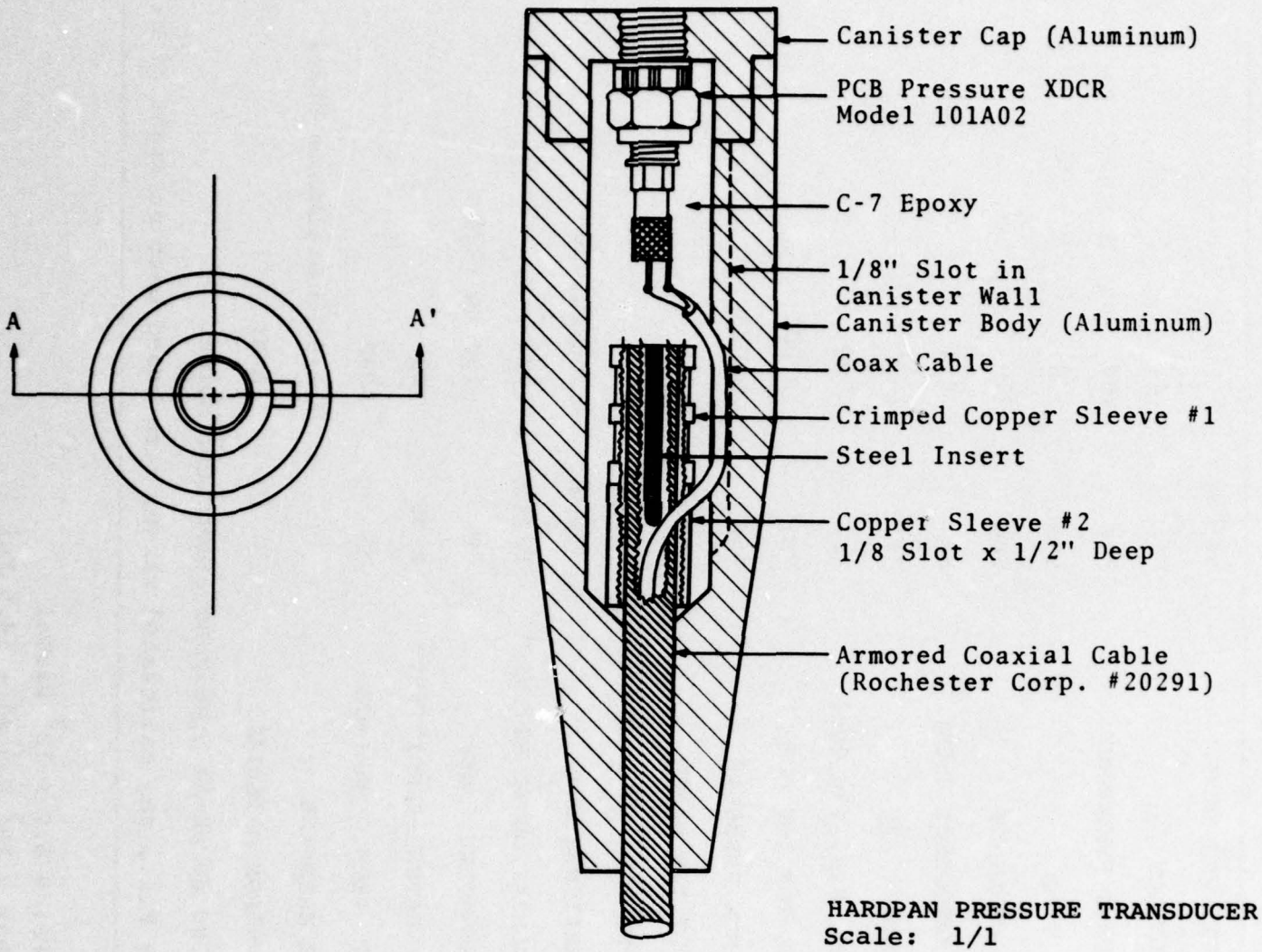

Figure 11. Air blast gauge assembly.

gauge element and firing the unit, a 250 mV negative step decaying back to zero in about 50 ms was created. Using the same Xenon source with a 6 mil (150 μm) thick cover of black tape (electrician's plastic type) over the gauge, the signal was reduced to about -12 mV with a 50 ms decay. However, with this covering the sun gun generated a 200 ms long drift to a negative peak of about 400 mV. This result suggested that the black tape is a very bad choice for protection since it absorbs incident radiation easily. A better choice would be a reflective cover. Thus by using two layers of aluminized mylar, 2 mil (51 μm) thick, with 1/2 mil (13 μm) aluminum coating, the impulse from the Xenon source was reduced to about -15 mV and the long term effect by the sun gun was only -25 mV in 200 ms.

The armored cable used to connect the gauges to the outside of the test bed is shown in Figure 12. The cable run from the test bed edge to the instrumentation van was an "Island 4" type furnished by the Air Force Weapons Laboratory (AFWL).

3.2 RESULTS

Times of arrival were obtained for all eight gauges and several provided useful details of the pressure history in the test bed cavity. For example, oscillations in the cavity pressure were recorded faithfully; Figure 13 shows that the time between peaks of the oscillation was about 2 milliseconds for gauge 917. Converted to pressure units, the raw data records are given in Figures A1 through A8 of Appendix A.

The most significant problem with these data is an apparent zero shift for six of the gauges at air and/or ground shock arrival. All the shifts were negative. To compensate for this problem, we applied a step-function correction to the data at shock arrival; the magnitude of this offset was chosen so that the gauge output at late times (150 to 450 ms after

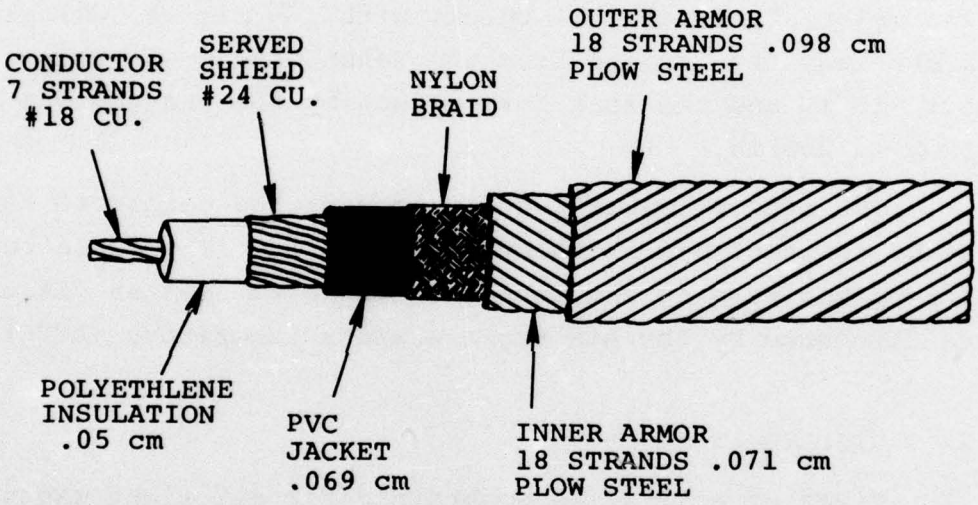

Figure 12. Construction of Rochester Corporation coaxial cable. Stock #20291.

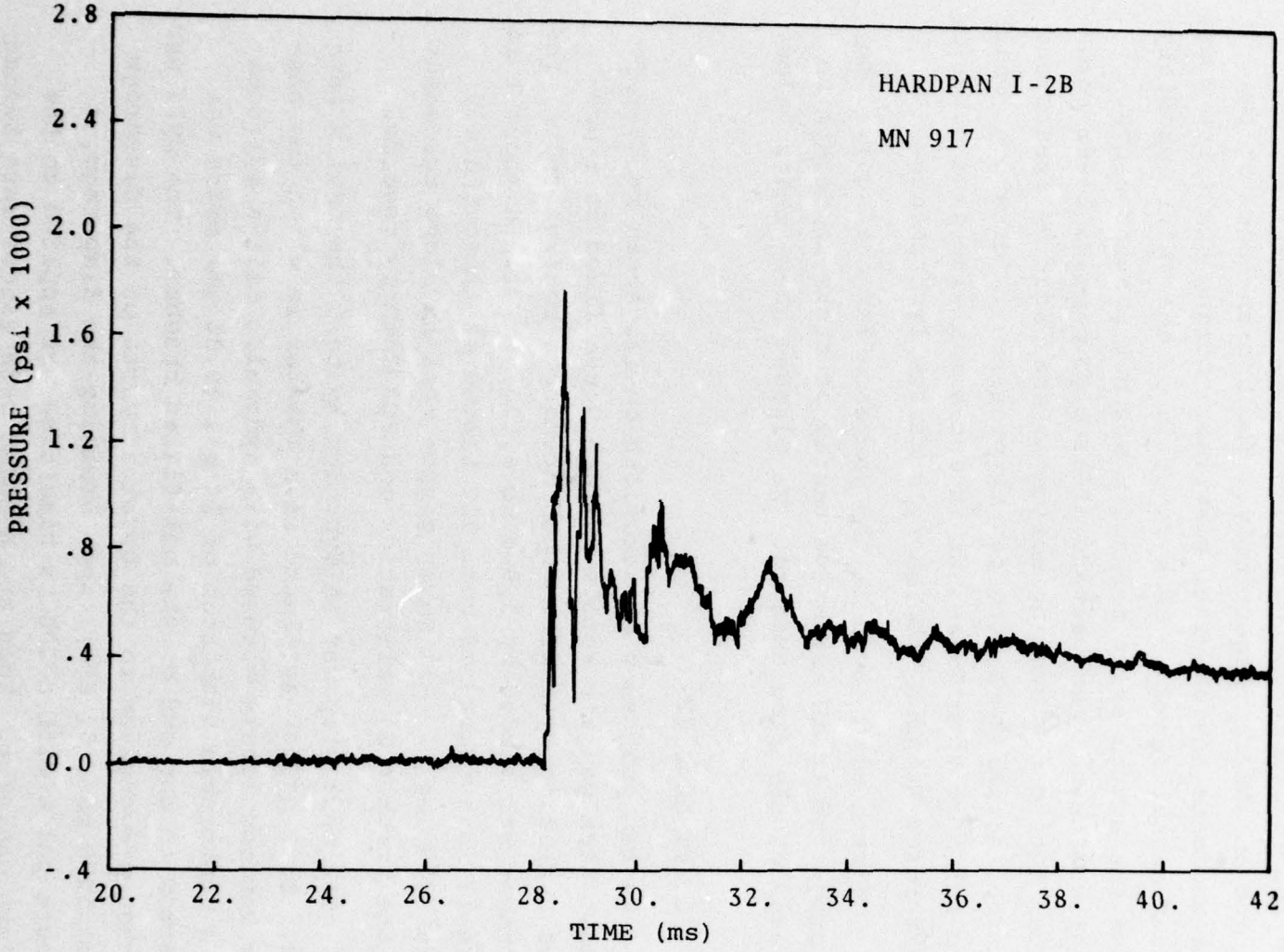

Figure 13. Quartz air blast record 917 time expanded to show cavity oscillations.

blast arrival) equaled the preshock level. In the worst case, this shift corresponded to -3.4×10^6 Pa (-500 psi). Figures 14, 15 and 16 are corrected records of worst case, intermediate and no shift, respectively. The broken lines on the graphs indicate the original baseline. During the first 2 ms, the peak signal seems to be a function of the shift, probably because the actual shift mechanism was not instantaneous. The units with the most severe offsets gave peaks lower than expected due to the bucking action of the negative excursions. After the initial 2 ms, the cavity pressure information, which lasted for more than 50 ms, is in agreement with data taken by the Air Force Weapons Laboratory's nearby instruments.

We recovered seven of the gauges after the shot. They were subjected to an extensive series of tests to determine the cause of the zero changes. We discuss these tests below.

3.3 SHIFT ANALYSIS

We ran post shot calibrations on all seven recovered gauges. Each gauge's active surface was affixed to a preloaded hydraulic cylinder. Upon opening a control valve, the instrument was loaded by 3,000 to 4,000 psi within about 1 ms. Figure 17 is a record of unit 912 tested at approximately 24 MPa (3500 psi). All seven gauges were in close agreement with the preshot S^3 calibration and PCB Company records.

The next step was to dynamically test the entire canister. Each gauge was placed in a chamber in which the canister was completely covered with hydraulic oil; a cylinder with a rupturable diaphragm of 14 mil (0.36 μm) brass was connected to one end of the oil-filled chamber. The cylinder was then pressurized to the burst strength of the diaphragm (about 5400 psi, 37 MPa); upon breaking the diaphragm, a pressure pulse with a 100 μs rise time was applied to the complete canister. When the HARDPAN I-2B gauges were tested

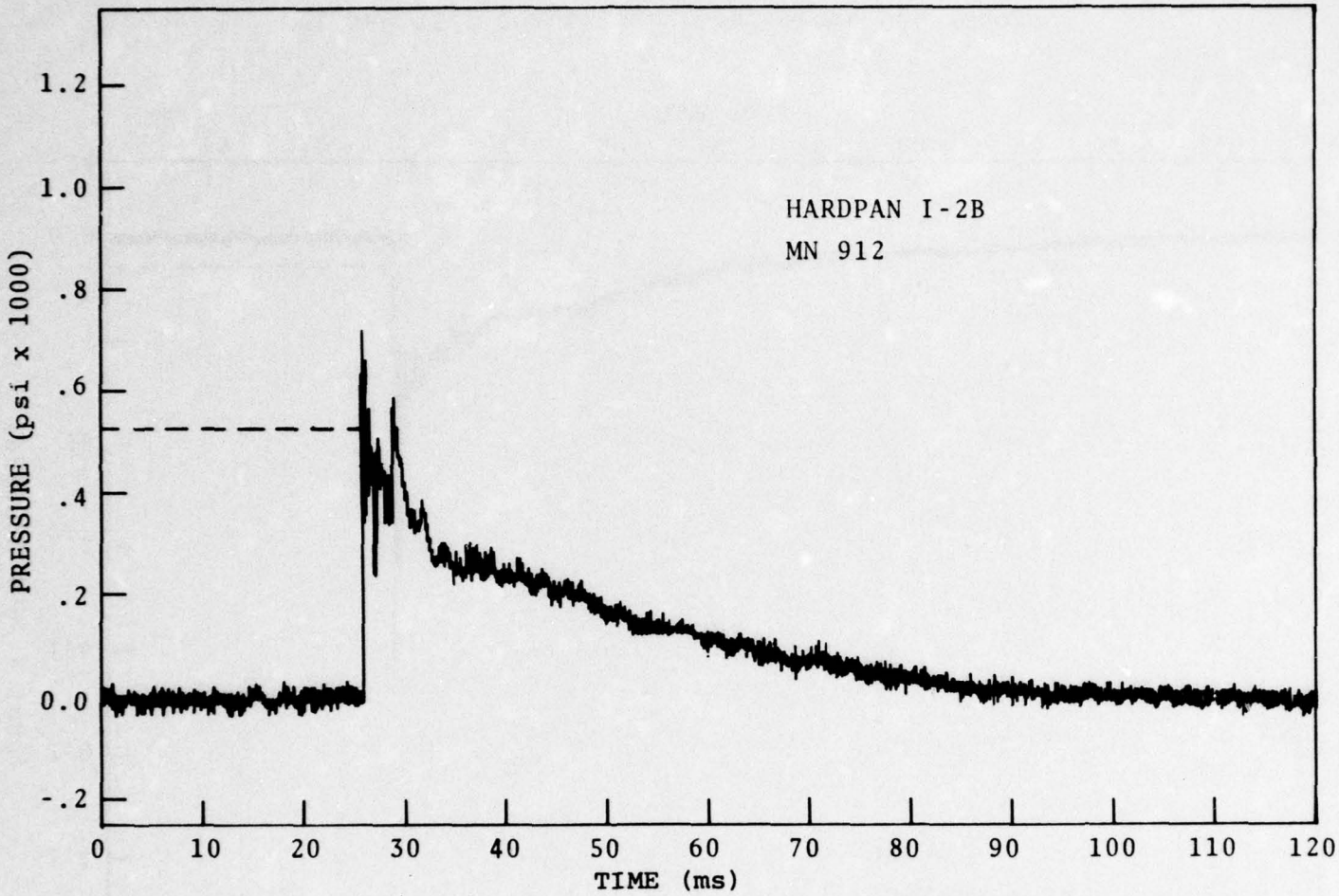

Figure 14. Quartz air blast gauge 912 record.

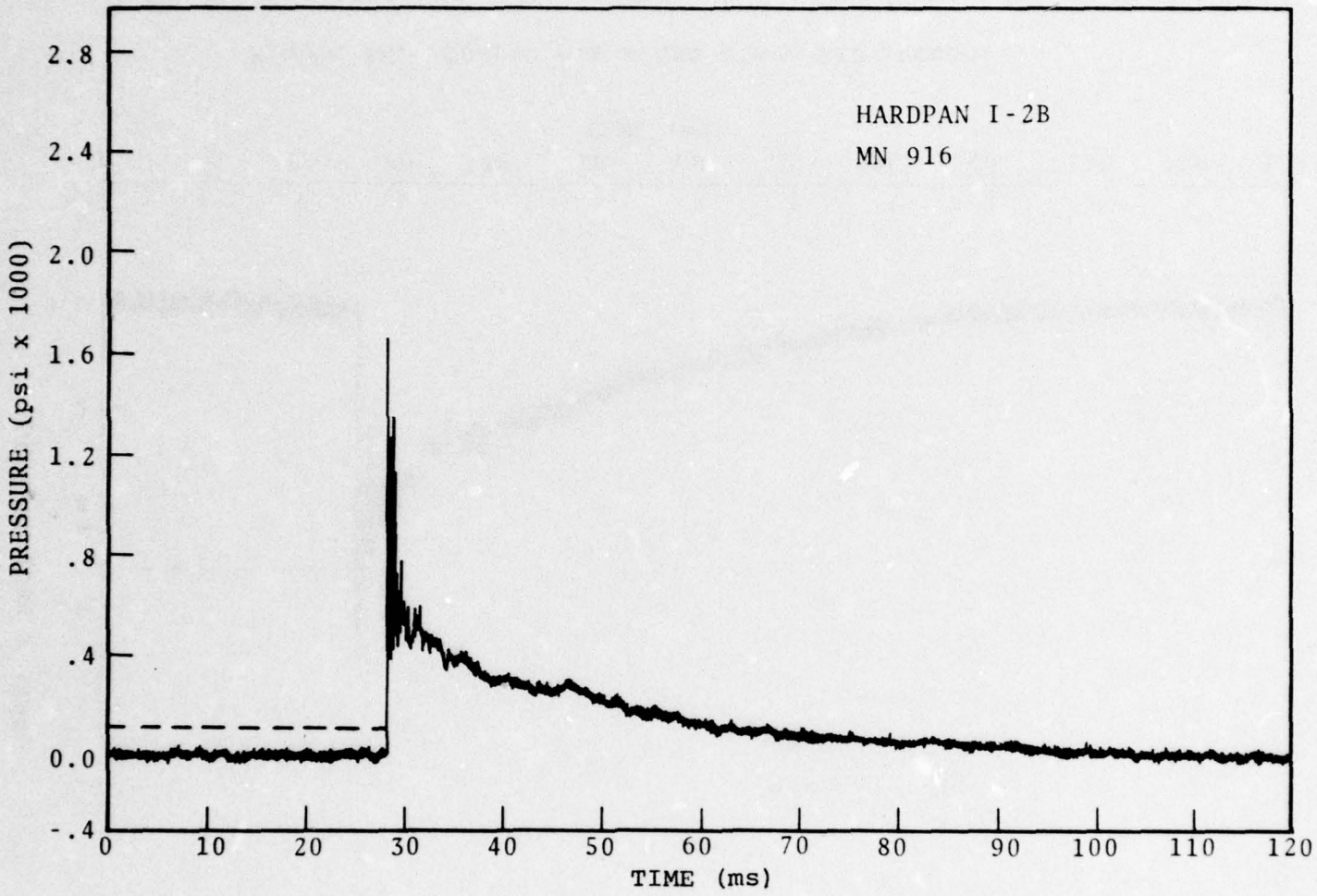

Figure 15. Quartz air blast gauge 916 record.

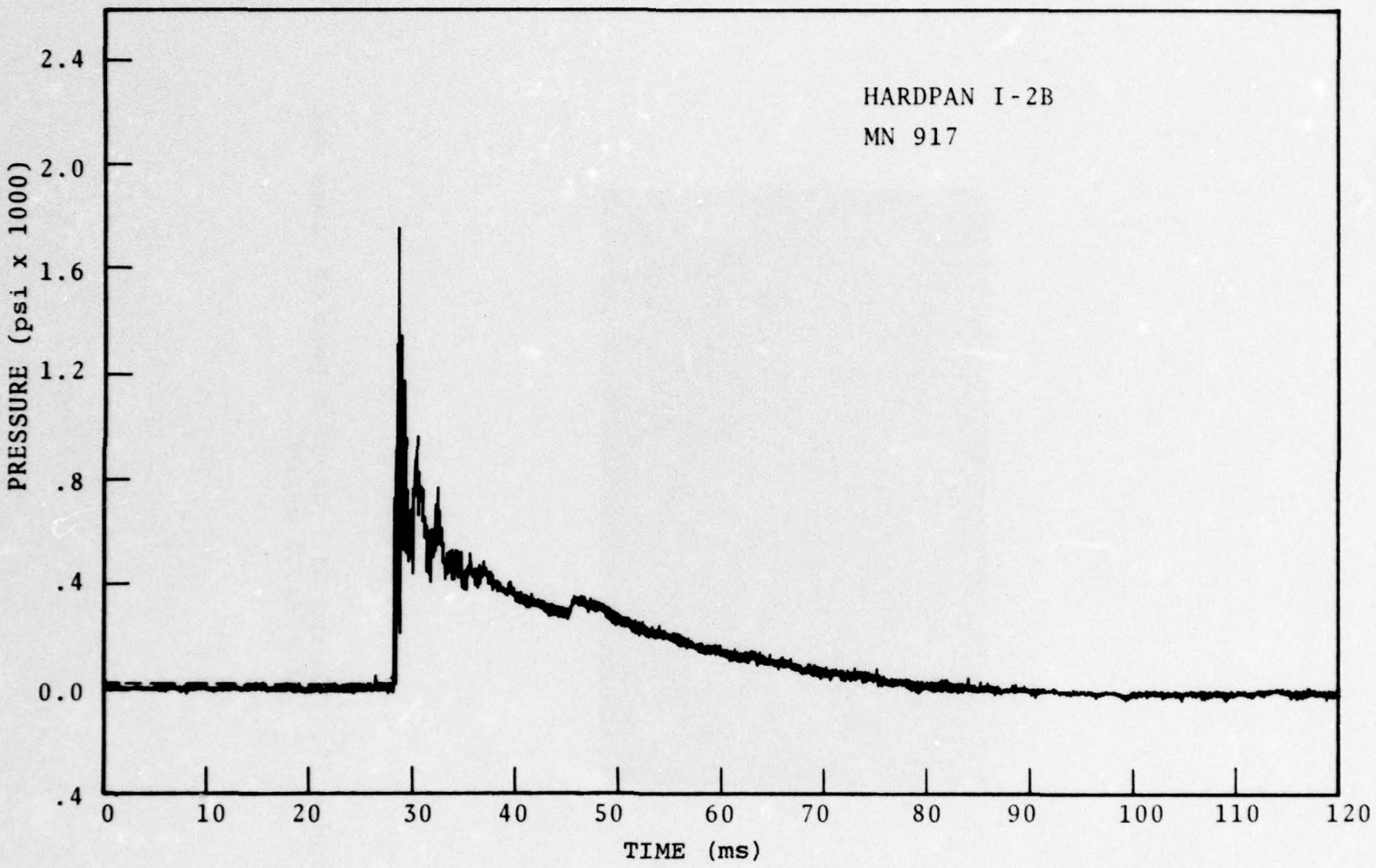

Figure 16. Quartz air blast gauge 917 record.

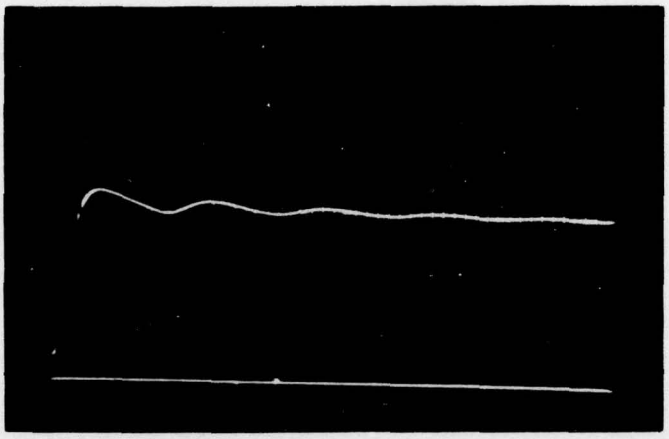

Figure 17. Record of hydraulic test of Gauge 912 (1 V/cm, 2 ms/cm).

in this manner, there was no indication of zero shift. All gauges responsed normally and gave correct pressure outputs.

In our laboratory experiments, the only mechanical way to cause a significant negative shift in the gauge output is by placing the armored cable on an anvil and striking it with a hammer; the resulting shift is comparable to that seen in the HARDPAN records, showing a time constant of some 2 to 3 seconds and a negative pressure of about 0.69 MPa (100 psi). Mr. Renick of AFWL informed us that the field records also showed a return to the original zero level in 2 to 3 seconds. Close inspection indicated the braided shield of the coax cable was being driven into the center conductor and momentarily shorting the gauge. Direct hammer strikes on the transducer or canister cause no such shifts.

In a further effort to determine the shift mechanism, two experiments with plastic explosives were carried out. The experimental setup consisted of a metal sphere with an inside diameter of about one foot. The HARDPAN I-2B gauge No. 269 was placed in the sphere along with its approximately 10 feet of armored cable. The cable was covered by four inches of "dirty" water* with the gauge canister just out of the water. A ball of C-4 explosive weighing 20 grams was centered in the sphere and detonated. A peak pressure of around 17 MPa (2500 psi) with a residual pressure of around 1 MPa (150 psi) (decaying to zero in about 10 seconds) was obtained. From this experiment there was no indication of a negative shift as seen in HARDPAN I-2B shot.

The second experiment was identical to the above except a 30 gram charge was detonated in hope of achieving a

---

*The water was drawn from the well at the Green Farm Test Site and soil was added to give it a murky appearance.

larger residual pressure. A pressure of about 24 MPa (3500 psi) peak was obtained and after one millisecond there was a shift in base line to a negative level equal to over 6.9 MPa (1000 psi). The negative "pressure" lasted approximately 10 seconds after detonation. The pressure pulse did recover exponentially over a time of 14.5 seconds and finally reached a positive level of 2.7 MPa (400 psi) before returning toward zero.

Our suspected mechanism for the zero shift is conductive water being driven through the shield and into possible pin holes or other weak points along the cable's dielectric, thereby causing a semi-shorting condition. In the laboratory a 2 kΩ resistor placed across the gauge cable will produce an apparent zero shift equal to 3.4 MPa (∿500 psi) negative.

3.4 CONCLUSIONS

The cavity pressure information is usable by the Air Force after the simple baseline shift corrections are applied. A series of post shot tests indicated that the gauge design is satisfactory. The internal electronics and canister gave no indication of breakdown. The gauge's ability to perform well in these tests lends credence to the cable fault theory. The reason for the zero shift has not been determined with certainty; however, as a result of the shift investigation the entire gauge package has been subjected to much more severe punishment than would be normal in a free-field test system checkout. We were able to reproduce the negative shift by shorting the gauge cable with appropriate resistances. We were also able to generate shifts when the cables, immersed in "dirty" water, were subjected to blast loading. Thus we suggest that the signal cables partially conduct to ground during pressure loading. This idea is supported by the fact that the HARDPAN shifts were proportional to the length of cable running approximately parallel to the airblast front in the test bed. As an example, two gauges (912 and 911)

with parallel runs of approximately 6.7 m (22 feet) each gave a zero shift of about -3.4 MPa (-500 psi). Two other gauges (913 and 914) with parallel runs of approximately 3.7 m (12 feet) each gave a zero shift of about -1.7 MPa (-250 psi).

We recommend that, in future experiments using an armored-type cable, a sleeve of rubber hose be drawn over the cable exposed to wet conditions. The hose would prevent moisture from entering the stranded armor shield and also serve as mechanical protection during fielding with heavy equipment in the test area.

SECTION IV

STRESS GAUGE INSTRUMENTATION

4.1 INTRODUCTION

We begin this section with a general review of techniques for the monitoring of stress in explosively-induced ground shocks. Then in Section 4.3, we discuss detailed features of those techniques that utilize piezoelectric transducers. In particular, we emphasize the properties and calibration of quartz (SiO_2) and lithium niobate ($LiNbO_3$) gauges.

4.2 STRESS GAUGE REVIEW

Stress gauges for recording nuclear and high explosive tests have been greatly improved during the last decade. We have undertaken a review of the currently popular gauges to compare their capabilities and to see if there are areas that could benefit substantially from further research and development. Only gauges of recent design or current use are discussed here. Previous work is reviewed by Rowland (1967) and Flanders (1964). Specifically, we are examining manganin, ytterbium, quartz, lithium niobate, and carbon gauges.

Manganin Gauges. Manganin was the first piezoresistive material widely accepted for use as a stress transducer. The early use is reviewed by Rowland (1967). It proved useful for laboratory experiments and for field experiments at relatively high stress levels (above 10 kbar*). The sensitivity is too low for practical field use much below 10 kbar. A more recent development in the use of mangain is for close-in measurements where the stress approaches a megabar. DeCarli (1974) has performed laboratory experiments using manganin above a megabar.

---

*10 kbar = 1 GPa = 10^9 Pa.

His work was specificially directed toward development of a field gauge for the megabar region. He fielded gauges on HUSKY PUP. Problems in the instrumentation alcove for that event precluded a complete field test of the system, but the gauge system appears feasible up to about a megabar. The main limitation seems to be shock-induced conductivity of available insulators.

Ytterbium Gauges. Ytterbium was studied, primarily at SRI (Keough, 1970), as part of an effort to find a piezo-resistive material with higher output than manganin for use in the sub-kilobar to 10 kbar range. Ytterbium was first fabricated as a laboratory gauge and used with gas gun experiments. The initial fielding for large shots occurred on DIAGONAL LINE and DIAMOND MINE (Petersen, 1973). Some useful data and some problems appeared from these efforts. Overall, the problems seemed solvable and thus the results were encouraging. In particular the DIAMOND MINE results showed the ringing of the cavity, although absolute amplitude was in doubt.

The gauges underwent a series of improvements and SRI, Sandia, PI and S^3 have used them in a number of field tests. Some of the better records have been obtained in 1000 pound experiments at NTS (Petersen, 1975; Smith, 1971; Grine and Coleman, 1974; Keough, 1974). Good records were also obtained on nuclear events such as DIDO QUEEN, HUSKY ACE (Smith, 1973), HYBLA FAIR (Kratz, 1975), and HUSKY PUP (Keough, 1976, private communication).

Gauge noise and survival problems were particularly evident on a number of large HE shots. It was often found that fairly good data were obtained up through the peak of the waveform but then the gauge either failed or gave a suspicious recording on unloading. Gauge construction has been considerably improved to strengthen the cable connection and

to reduce the possibility of unwanted strain signals due to bending of the element. With these improvements, excellent records were obtained in 1975 for PRE-DICE THROW (Rosenberg, et al., 1976, report in preparation).

Ginsberg (1973) of SRI has reported a detailed calibration study of ytterbium gauges using gas gun techniques. His data are used as the basis for reducing gauge data. Data reduction is not simple because the piezoresistivity of ytterbium is nonlinear and shows hysteresis on stress release. The response in 1-D strain is different from the hydrostatic response. Ginsberg's data suggest that, for general field use, the intrinsic uncertainty in calibration of the gauge can be kept below 10 percent. With the selection of all strain elements for a test from the same ytterbium lot, care in preparation and other cautions that Ginsberg discusses, the variations in sensitivity within a group of gauges can probably be pushed below 5 percent. This assumes however that the gas gun calibrations are appropriate for the field tests which have lower strain rates. This assumption has never been satisfactorily checked. A few static 1-D tests agree reasonably well with the gas gun data, suggesting that, at least for the initial loading, the calibration data are valid. However, as gauge construction is improved so that we can record field data through the entire stress release, the validity of the calibration must be confirmed, especially if the waveform shows multiple bursts, reflections, or other significant structure.

A preliminary attempt was made to perform drop-bar calibrations (see Section 4.6) on ytterbium at S^3. Fair agreement with Ginsberg's calibration was seen. Further technique development would be necessary to enable us to perform well-controlled drop-bar tests.

The ytterbium gauge has an advantage over many other gauges in field use in that it is a low-impedance system,

usually with no down-hole instrumentation. Figure 18 shows a sketch of the system. Electrically, it consists of the ytterbium grid, typically between 5 and 50 ohms, copper leads connecting to the field cable (often RG213), and a power supply in the recording trailer. The supply is often in the form of a modified Wheatstone bridge. At shot time, a constant voltage source, typically 100V, is applied to the bridge. The network remains balanced until the stress wave loads the grid, increasing its resistance. The unbalance of the bridge is recorded as a voltage-time waveform with oscilloscopes or a tape recorder.

The system described above is very simple, but it runs into difficulties for stress levels below about a kilobar. Both the unwanted bending signal and the heating of the gauge by the power source causes a drift that is signficant compared to the true signal. Keough (1974) describes a carrier system that he has used successfully at stresses as low as 0.3 kbar to overcome the heating problem. Excitation was with a 40-kHz oscillator, which gave better signal-to-noise discrimination, reduced power dissipation, and allowed continuous operation (i.e., no power supply triggering).

Lithium Niobate Gauges. Lithium niobate gauges have been developed primarily by Sandia. The active element of the gauge is a disc of lithium niobate, a synthetic single crystal ferroelectric material. Its piezoelectric sensitivity is an order of magnitude higher than that of quartz and it has a very high Curie point (1150°C). As in the quartz gauge, the crystal is used as a charge source with the charge at the disc electrodes being proportional to the average stress over the area of the disc.

Sandia has fielded versions of these gauges on a number of large tests, including ESSEX (Vortman & Beyeler, 1974), HYBLA FAIR, and the Rock Springs oil shale experiment (Reed, 1975). Some good waveforms have been recorded; however, in the few tests where quartz, ytterbium and lithium

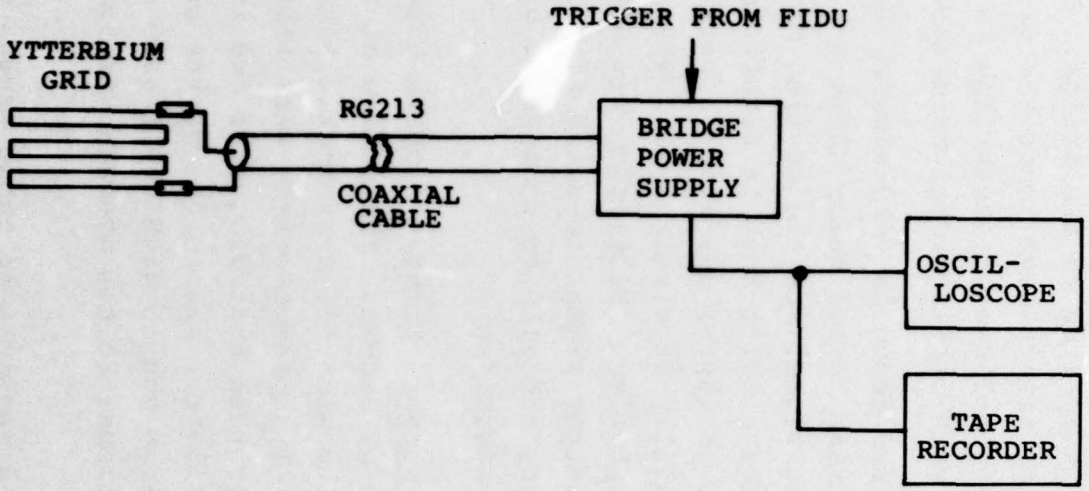

Figure 18. One channel of ytterbium gauge and instrumentation (Smith, 1971).

niobate gauges have been used together, the magnitudes have not always been in agreement. This may reflect insufficient data, a calibration problem, or general packaging and fielding problems common to all gauge types, but it should be investigated more thoroughly. Sandia is fielding different gauges together as much as possible (R. P. Reed, private communication, 1976). A more complete review of lithium niobate gauge technology begins in Section 4.3.

Quartz Gauges. The majority of the development and fielding of the quartz gauge has been done at S^3 (e.g., Kratz, 1975; Glenn, 1973). The most complete work on construction and calibration is in the final report on Contract No. DNA001-75-C-0184. A more detailed review of quartz gauge techniques is given in Sections 4.3 to 4.6.

Carbon Gauge. The use of the carbon gauge has recently been documented in detail by Nauman, et al., (1975). The gauge is mainly used for high x-ray environments, where it can withstand 50 times the fluence of the quartz gauge and 200 times the fluence of the manganin gauge. The carbon gauge has seen a lot of use in measurement of radiation-induced pulses in underground tests; ETI has fielded over 100 gauges.

There are several different types of carbon gauges. The element for the EG&G gauge (now made by Dynasen, Inc., Santa Barbara, California) is produced by dipping a 0.0025 cm Kapton backer into aqueous carbon slurry, leaving a thin layer. After heat treatment, beryllium or copper leads are vapor deposited. The carbon is then scraped away to the desired size and resistance, and the gauge is encapsulated with epoxy and Kapton.

The ETI gauge is designed without Kapton in front to give a faster response. The carbon element is the MystR composition of Waters Manufacturing. The element is connected to thin beryllium leads with carbon bonded epoxy and insulated on the back by a Kapton sheet.

The SRI gauge was made with pure carbon evaporated on a boron nitride substrate. However, the gauge failed, probably by cracking of the element, at 26 cal/gm x-ray deposition. Development of this gauge was not continued.

Several modifications of the EG&G and ETI gauges have been made to achieve smaller size and lower noise operation.

Calibration has been performed mainly by gas gun tests (Horning and Isbell, 1975). A nonlinear relationship is seen between pressure and resistance change with a slight offset between loading and unloading. The different gauge types have separate calibration curves. For example, the ETI gauge shows a resistance change of -50 percent at 45 kbar and -25 percent for 10 kbar. The small EG&G gauge shows -50 percent at 23 kbar and -25 percent for 7.2 kbar. Least squares fits to the various calibration curves show standard deviations in pressure of 7 to 10 percent.

4.3 PIEZOELECTRIC STRESS GAUGES

In this section, we discuss the use of piezoelectric crystals for the measurement of stress components in ground motion. In practice, the only field-proven instruments have been those sensitive to a principal component of the stress tensor. Quartz has been the material of choice because of its availability, uniformity and linearity. Recently, workers at Sandia appear to have had some success using lithium niobate. This crystal can be cut so that it responds to the mean stress, i.e., isotropic pressure.

Aside from the selection of the transducing medium, the most important consideration is packaging. The gauge must protect the crystal and signal conductors from moisture, pressure and acceleration effects. We discuss below the characteristics of quartz and $LiNbO_3$, package construction, and calibration.

Grine (1975) has recently summarized field applications of a hardened quartz instrument. Reed (1975) discusses one instance of the use of lithium niobate in the field.

4.4 CRYSTAL CHARACTERISTICS

The piezoelectric response of a cut crystal disc depends on the orientation of the cut with respect to the intrinsic axes of the crystal. For X-cut quartz, the charge density P_x (nanoCoulombs per cm^2)* induced across the disc's faces is given by

$$p_x = -23\sigma_{xx} + 23\sigma_{yy} - 6.7\sigma_{yz} \tag{21}$$

where the stress components are in kilobars. Various references imply that these numerical coefficients are accurate to ± 0.5 $nC/cm^2/kB$. Note that this cut has a uniquely zero response to the mean stress and no response to shears on the crystal faces. If a large shear sensitivity is needed (as in some accelerometer designs), the Y-cut is useful:

$$p_y = 46\sigma_{xy} + 6.7\sigma_{xz}. \tag{22}$$

Lithium niobate is a somewhat more complicated crystal than SiO_2, quartz. For $LiNbO_3$, the piezoelectric coefficients may be written as a matrix:

$$\begin{array}{c} \\ P_x \\ P_y \\ P_z \end{array} \begin{array}{c} \begin{array}{cccccc} \sigma_{xx} & \sigma_{yy} & \sigma_{zz} & \sigma_{yz} & \sigma_{xz} & \sigma_{xy} \end{array} \\ \begin{pmatrix} 0 & 0 & 0 & 0 & 692 & -416 \\ -208 & 208 & 0 & 692 & 0 & 0 \\ -8.5 & -8.5 & 60 & 0 & 0 & 0 \end{pmatrix} \end{array} \tag{23}$$

*1 $nC/cm^2/kB = 10^{-13}$ Coulomb/Newton.

Unfortunately, these numerical values are not so precisely known as those of quartz. The numbers given here are based on a compilation current to 1972. Recent, more accurate measurements show significant differences. Graham and Jacobson (1973) claim that for Z-cut discs in uniaxial stress,

$$P_z = [(73.3 \pm 0.5) + 0.23\sigma_{zz}]\ \sigma_{zz} \tag{24}$$

and that in an isotropic pressure field, p in kilobars,

$$P_z = [(63.1 \pm 0.1) + 0.88p]p \quad . \tag{25}$$

Note that there are small nonlinearities in these responses; in fact, quartz also displays some comparable nonlinearities (Graham, 1974).

Neglecting the uncertainties in the numerical values, $LiNbO_3$ does have several unique properties. For a Z-cut crystal, it will respond to pressure. As a slight complication, however, $LiNbO_3$ shows a pyroelectric sensitivity of 4 $nC/cm^2 °C$ along the z axis. Thus if the crystal's sides are isolated, its complete response along the z axis is

$$P_z = 73\sigma_{zz} + 4\Delta T \tag{26}$$

where ΔT is any temperature change occurring during the measurement interval. Of course, for a buried instrument measuring transient stresses, this temperature response should be negligible.

For a properly cut $LiNbO_3$ crystal, the output level can be greatly increased over that of quartz. Thus with a 39 degree rotated Y cut disc (Cady, 1964), the charge density is given by

$$P_y' = -165\ \sigma_{xx}' + 377\sigma_{yy}' - 173\sigma_{zz}' + 2\sigma_{yz}' + 2.5\Delta T \qquad (27)$$

where we have used Graham's values for the z axis piezoelectric coefficients and neglected the nonlinearity terms. (The primed quantities in Equation (27) are taken with respect to the rotated reference frame in which y' is perpendicualr to the disc's faces.) If the crystal's sides are isolated, the uniaxial response is 16 times that of quartz; to within ± one degree, this cut minimizes the shear response, σ_{yz}'.

For a 163 degree rotated Y-cut $LiNbO_3$, the shear response is dominant for a properly isolated crystal:

$$P_y' = 197\sigma_{xx}' + 4\sigma_{yy}' - 183\sigma_{zz}' - 673\sigma_{yz}' - 1.2\Delta T \qquad (28)$$

Note the low response to the compressional stress, σ_{yy}'. Perhaps a gauge package could be designed to take advantage of this cut, allowing ground shear stresses to be measured. With a suitable set of electrodes on the faces of this cut and the addition of a seismic mass, a rotary accelerometer could also be fabricated.

4.5 PACKAGING

While quartz is extensively used in a variety of commerical force and pressure gauges, these packages are rarely appropriate for the rugged environment of ground motion studies. A field proven configuration, based on a design originally developed by Kratz and his group at Gulf Radiation Technology, is shown in Figure 19. The sensing element, X-cut quartz, is sandwiched between two Lucalox (aluminum oxide) discs for insulation. Thin copper foils on the faces of the quartz pick up the stress-induced charge. An aluminum piston communicates the external stress to the quartz. An O-ring

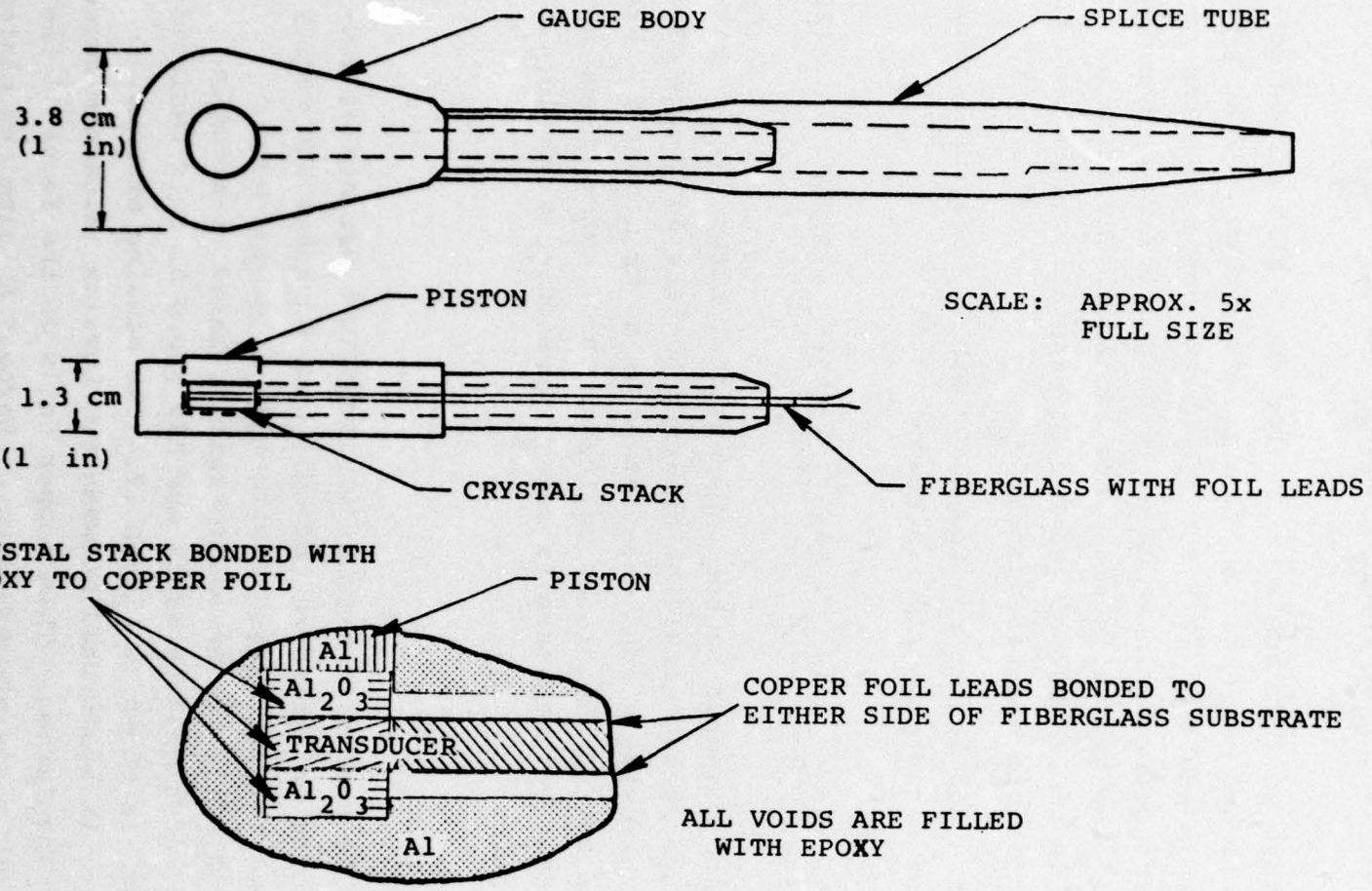

Figure 19. Quartz stress gauge (1 in. = 2.54 cm).

around the piston prevents water leakage and a thin external coat of epoxy further seals the unit. The perimeter of the quartz does not touch the gauge body; this isolates the transducer from side stress, σ_{yy}. If a long cable run is needed between the gauge and the recorder, then a FET source follower is located near the package; this circuitry serves as an impedance buffer to match the high impedance crystal to a long cable. The cables used are either encased in protective tubing or are armored well-logging types with a high resistance to tensile and shear failure.

This gauge system has proven reliable in field applications to stresses of 0.5 GPa (5 kB) and accelerations of 10^7 m/sec^2 (one million g's). Waveforms with risetimes of 5 μs are faithfully recorded and the acceleration sensitivity, 1 Pa/m/sec^2, is usually negligible.

We have recently had some success in making similar gauges with the substitution of 36 degree Y-cut* $LiNbO_3$ for quartz. Lithium niobate does seem to be more vulnerable to thermal shock than quartz; thus all fabrication steps including epoxy cures should be carried out at room temperature.

Reed (1975) at Sandia has reported on the use of Z-cut $LiNbO_3$ for field use. In the Sandia design, the crystal is sandwiched between 3 mm thick fiberglass boards in a paddle-shaped geometry; the configuration is similar to that used for ytterbium stress instruments. This design provides a gauge responding to mean stress, i.e., pressure. Packages of this form are apparently available from Specialty Engineering Associates of San Jose, California.

---

*The 36 degree cut is currently popular for electro-optic applications. At the time of our purchase, it was most readily available. It is not optimum with respect to minimizing the shear response. For the 36 degree cut, Equation (27) becomes

$$P'_y = -171\sigma'_{xx} + 389\sigma'_{yy} - 181\sigma'_{zz} + 56\sigma'_{yz} + 2.5\Delta T \ . \quad (27')$$

4.6 CALIBRATION

The piezoelectric coefficients of isolated quartz and $LiNbO_3$ crystals have been carefully determined in laboratory studies. However when the transducing element is incorporated into a fieldable package, the gauge sensitivity may differ from that of the bare crystal. The strength and configuration of the packaging materials may prevent the sensor from "seeing" the true external stress field. It is well-known that this potential problem is involved in the choice of a grout for field installation of any stress instrument.

When possible, the entire gauge should be calibrated. The testing should be at the stress levels, risetimes and durations expected in the field. Repeated response checks at several different pressures can also serve the very valuable function of weeding out marginally constructed units. Fluid-filled chambers impulsively loaded by a bursting diaphragm may be suitable for testing pressure sensing types; we discussed such tests in Section 3.3.

For checking instruments with uniaxial response, we have had good success with a drop bar apparatus. Glenn (1973) discussed the basic design of this system. A tapered, meter-long rod of plastic, aluminum or steel is dropped from heights of 0.1 to 3 meters onto the gauge's piston. The gauge body is firmly supported on a massive, rigid surface. By measuring the bar's velocity just before and just after the impact with a light-beam system, we can use conservation of momentum to derive the gauge's sensitivity:

$$K = A_C C \int_0^\tau V \, dt / M_B \, (S_i + S_r) \qquad (29)$$

where

K = sensitivity in Coulomb per Pascal,

A_c = area of the sensing crystal in m^2,

C = capacitance across the signal leads in Farad,

V = the signal voltage during the impact (integrated over the duration τ of the collision), in volts,

M_B = mass of dropbar in kg,

S_i = speed of bar at impact in m/sec,

and

S_n = speed at rebound.

The duration of the collision is the time required for a finite amplitude stress wave to propagate up and down the bar,

$$\tau = \frac{2L}{c_\omega} \tag{30}$$

where L is the bar length and c_ω is the wave speed. For our bars, the latter is usually smaller than the speed of sound in the bar material, see Table 3. We find the peak stress of the impact can be predicted to within ± five percent from the simple, one-dimensional shock relation

$$\sigma_{Peak} = \frac{A_B}{A_C} \rho_B c_\omega S_i \propto \sqrt{H} \tag{31}$$

where

A_B = cross-sectional area of the bar,

H = drop height

and

ρ_B = bar density.

Table 3. General Features of Dropbar Calibrator.

Drop Bar M_B, kg	τ Impact Deviation μs	c_w m/s	c_s Sound Speed m/s	Peak Stress* for 1 meter Drop kBar
Lucite 1.23 m .406	1200 ±10	2.06×10^3	2×10^3	0.41
Aluminum 1.25 m .959	522 ±3	4.78×10^3	5.1×10^3	2.45
Steel 1.32 m 3.114	635 ±15	4.16×10^3	4.9×10^3	7.2

*1 kbar = 100 MPa.

With careful design of the apparatus, the bar will be in free-fall, and the peak stress will be proportional to the square root of the drop-height. Tapering the bar provides stress rise and fall times of about 100 μs.

We have recently constructed a set of the stress gauges using various cuts of quartz and lithium niobate. The X-cut quartz discs, 9.53-mm-in-diameter by 1.58-mm-thick, were obtained from Precision Crystal Laboratories, Santa Monica, California. Similar sized $LiNbO_3$ samples were purchased from Specialty Engineering Associates. All the gauges were fabricated by the same person. We subjected each gauge to at least fifteen dropbar calibrations, spanning a stress range of 0.03 to 0.4 GPa. Table 4 gives the results. In general, both types of crystal performed well. The sensitivities of the quartz gauges range from 91 to 100 percent of the ideal, Equation (21); the lower values may reflect some stress losses through the O-ring that serves as a moisture barrier. For the 36 degree Y-cut $LiNbO_3$, the responses range from 85 to 91 percent of the ideal, Equation (27′); it should be remembered, though, that the "true" sensitivity of $LiNbO_3$ is not yet perfectly known. Nearly all the gauges show sensitivities reduced by 4 to 7 percent at stresses below 0.07 GPa. This may reflect some anomalous behavior of the Lucite dropbar or stress losses through the O-ring.

A slight amount of hysteresis is also evident for all the units. After the impact, the signal output remains at some small fraction of the peak signal. From test to test, this zero shift varies by factors of two or three in magnitude; it is almost always positive in sign. The percentage shift is usually largest for the first few shocks of a newly built gauge; it does not appear that continued testing will reduce the hysteresis to undetectable levels. Unlike the situation with accelerometers (Section 5), the integral of stress is rarely needed with high precision, so this low level of shift can be neglected.

Table 4. Summary of Dropbar Calibrations.

Type	ID	Response at 0.2 GPa (x 10^{-13} C/N)	Average Zero Shift, % of Peak Stress
X-Cut Quartz	491	20.8 ±0.4	0.9
	492	22.5 ±0.4	0.2
	493	21.3 ±0.4	0.3
	494	22.9 ±0.4	0.7
36° Y-Cut $LiNbO_3$	495	330 ±6	1.7
	496	354 ±6	4
	502	348 ±6	1.4
	503	330 ±6	1.0
163° Y-Cut $LiNbO_3$	500	3 ±1	
	501		
	504		
	505		
	506		

Based on a limited amount of experience, we would recommend that lithium niobate in this gauge configuration not be used above 0.5 GPa. A few dropbar tests at this level led to fracture of the crystal.

Ideally, the X-cut quartz and (to a lesser extent) 36 degree Y-cut lithium niobate gauges should not be sensitive to shear forces on the piston. On the other hand, an instrument incorporating 163 degree Y-cut $LiNbO_3$ should be very sensitive to shear. To check these assumptions, we made several gauges of the latter type. In dropbar calibrations, the 163 degree type units gave very low responses consistent with the prediction of Equation (28). Then all the gauges were tested for shear response on the S^3-DNA rotary viscometer.

This device consists of a 1.27 m diameter steel wheel; it can be spun at rates from 0 to over 20 rpm. The gauge under test is mounted with its piston parallel to the perimeter of the wheel. Within a period of 20 ms, the gauge is pushed into contact with the wheel for a duration of 150 to 200 ms and at normal stresses of 0.05 to 0.2 GPa. Quartz load cells (Kistler Model 923F2) monitor the radial and tangential forces that the piston exerts on the spinning wheel. The total gauge signal may be written as

$$G \equiv \text{Gauge Signal} = \frac{F_R S_N}{A_C} + \frac{F_T S_S}{A_C} \tag{32}$$

where

F_R = radial force from load cell,

A_C = area of piston, 0.713 cm^2,

S_N = gauge compressive sensitivity from dropbar calibration,

F_T = tangential force from load cell,

and

S_S = gauge shear sensitivity to be determined.

In practice, we found that spin rates above a few rpm should not be used; otherwise, excessive heat is generated at the piston's surface.* Figures 20 and 21 give examples of the shear test results. For the quartz and 36 degree $LiNbO_3$ type instruments, the shear sensitivity is less than 15 percent of the compressive response,

$$S_S < S_N/15 \text{ for quartz and 36 degree } LiNbO_3 \quad .$$

This upper limit result is due to the ± 5 percent uncertainty in the calibrations of the load cells and the low keep "level" of the tangential force achievable for an aluminum surface sliding on steel.** It is also difficult to precisely determine the shear sensitivity of the 163 degree Y-cut $LiNbO_3$ gauges. However, the prediction of Equation (28) is consistent with our data to within ± 25 percent. If the gauge is rotated so that it experiences a shear stress transverse to its sensitive direction (σ'_{xy} versus σ'_{zy}), the observed signal output is reduced by a factor of over five. More work would be needed to make the rotary viscometer into an accurate shear calibrator.

---

*As an alternative, the contact duration could be reduced.

**We remind the reader that the coefficient of kinetic friction, defined as the ratio of the shear force over the normal force, is nearly independent of the relative velocity of the two materials; in fact, the kinetic friction decreases slightly as the velocity increases. Thus the maximum achievable shear stress for our setup is limited by the maximum permissible normal stress of the gauges, ∿ 0.4 GPa.

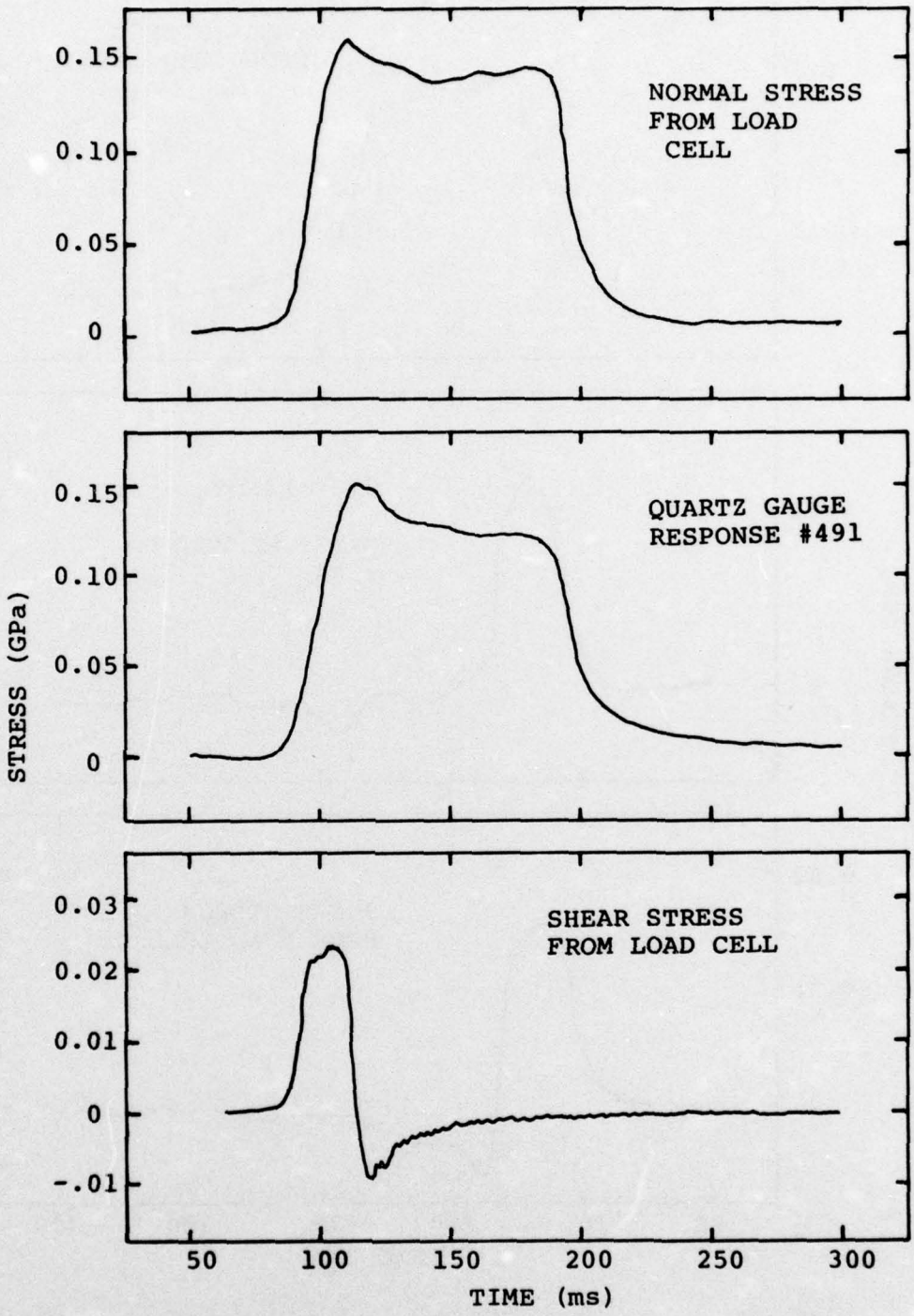

Figure 20. Example of shear sensitivity tests for X-cut quartz gauge. Wheel speed 2 rpm.

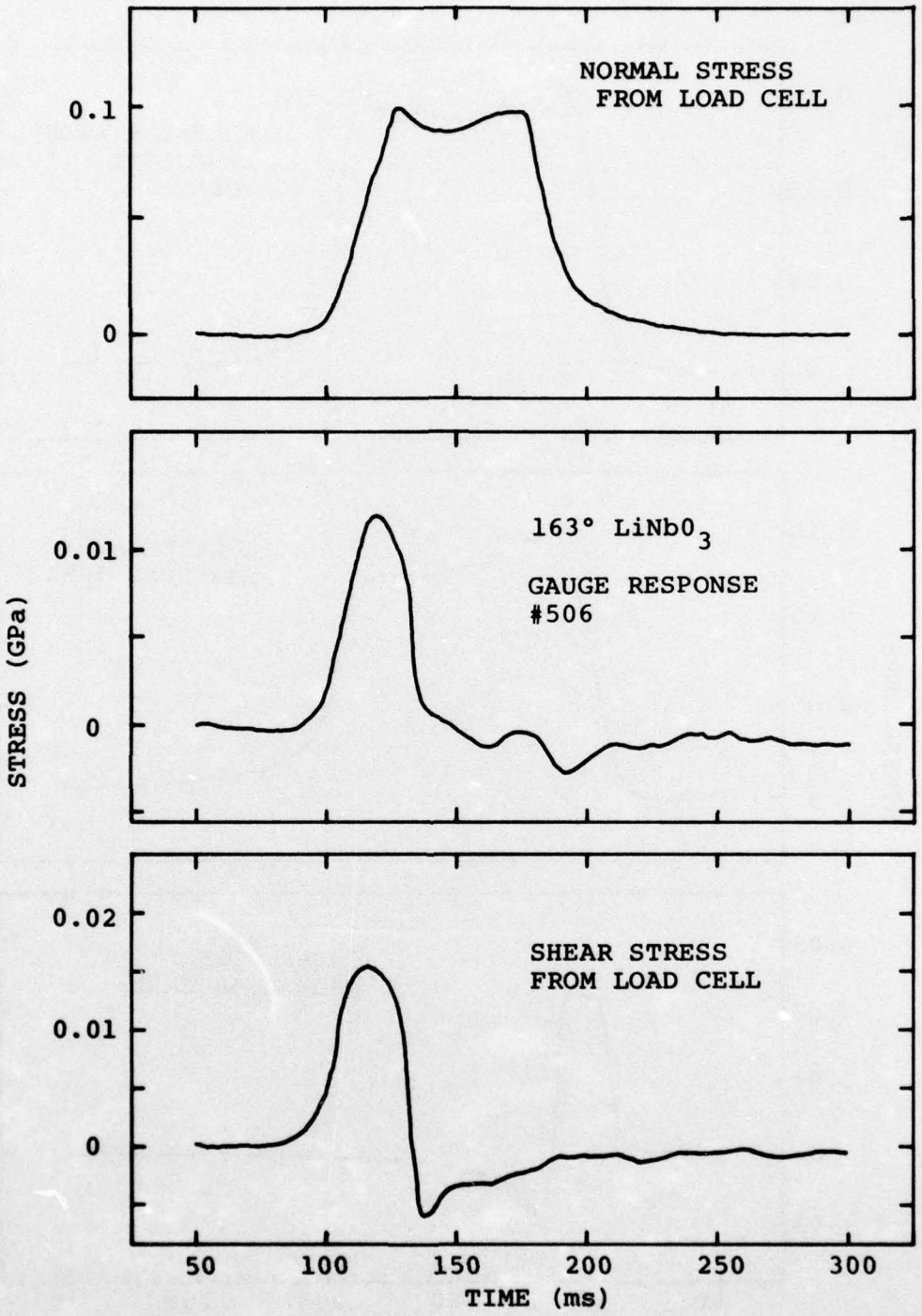

Figure 21. Example of shear sensitivity of 163° Y-cut $LiNbO_3$. Wheel speed 2 rpm.

SECTION V

ACCELEROMETER ZERO SHIFTS

5.1 INTRODUCTION

Almost all transducers are subject to some hysteresis. After a significant measurand input is removed, the signal level does not return to its former "zero" level. For example, the output of a quartz stress gauge will correspond typically to a ± 10^5 Pa (1 bar) pressure after receiving a one ms, 10^8 Pa (1 kbar) stress pulse; see Section 4.6. When the quantity of interest is the measurand, such small zero shifts may usually be neglected. In the case of ground motion studies, particle velocity is often of prime concern, but few transducers directly respond to velocity. Then it is often necessary to field an accelerometer and integrate, electronically or numerically, the signal. In this situation, a ± 0.1 percent zero shift can lead to great errors in velocity especially if long time intervals are needed.

Based on a sample of 14 accelerometers in field use*, we previously (Coleman, Ginn and Grine, 1975) observed typical zero shifts of 0.5 percent in acceleration, i.e.,

$$\frac{\text{(Slope of Velocity Signal Post Shock)}}{\text{(Peak Acceleration)}} \sim 0.005.$$

This represents a "dc" or long term shift. In addition, there appeared to be a time varying ("ac") shift; the post shock velocity, when extrapolated back to the shock beginning, was significantly different from zero, see Figure 22.

---

*Each transducer, combined with a rugged electronic integrator, was packaged into a field unit with an output signal proportional to velocity.

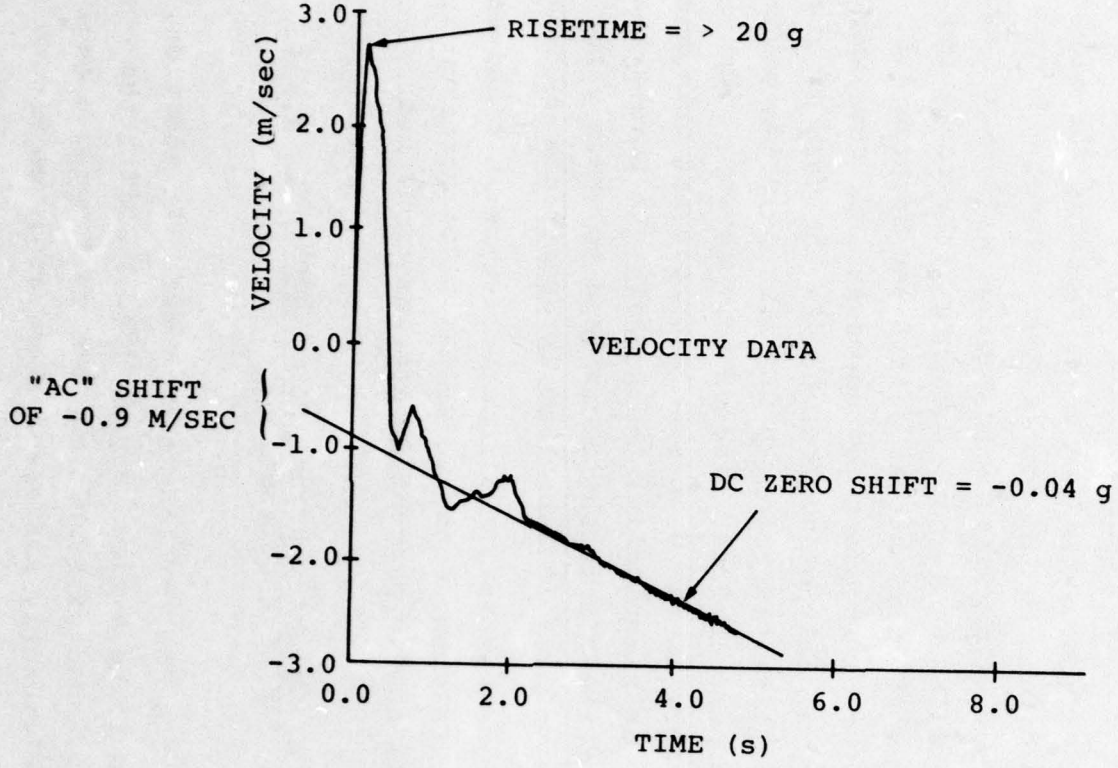

Figure 22. Example of "ac" and dc zero shifts. Accelerometer is rated at 250g. Dc shift is 0.2%.

In the laboratory, detailed testing of three isolated accelerometers reproduced these observations. We also noted that after subjecting the transducers to several hundred shocks, the average zero shift decreased by factors of three or more. Thus an "aging" or "exercising" process led to improvements in the accelerometers' performances. During the period covered by the current report, we have continued to study the zero shift problem.

5.2 RESULTS

In our recent work, we addressed ourselves to three questions. Is the "aging" permanent? Does the "aging" depend on the ratio of test level to peak rating? (The laboratory tests occurred at levels of about 2×10^4 m/sec^2 (2000 g's); the accelerometers were rated at peaks of 5×10^5 m/sec (50,000 g's) or more.) Is the time varying zero shift related to the dc shift?

Shifts of a few tenths of a percent are not easy to detect in direct oscilloscope or analog recordings of accelerometer data. In our previous work, we used a carefully designed electronic integrator to make the shifts measurable. We now are using a digital recorder with 12 bit (one part in 4096) resolution to directly monitor the accelerometer and velocity signals. Figure 23 shows our data system. The contents of the recorder's memory are readily placed on a digital magnetic tape and processed by a large computer. The agreement between numerically and electronically integrated acceleration data is good.

With respect to the first question, it appears that the aging is permanent. Two of the three original test accelerometers are still usable. A year after their initial exercising, their performances remain good. Table 5 summarizes the history of their hysteresis effects. Note that each

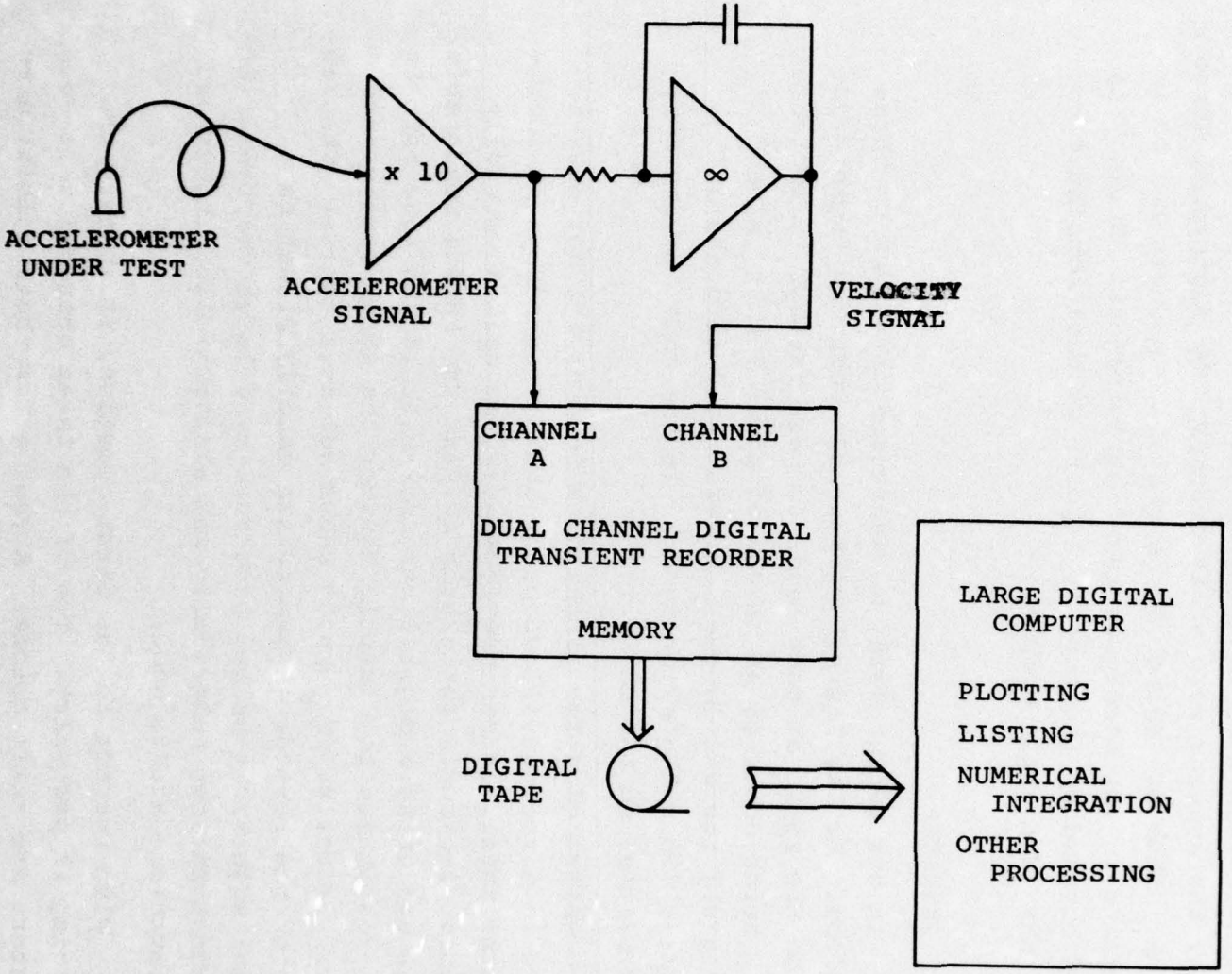

Figure 23. Recording system for accelerometer zero shift studies.

Table 5. Summary of Mean dc Zero Shifts of Accelerometers at 2×10^4 m/sec^2 (2000 g) Test Level.

Accelerometer (S.N.)	Date Mfd.	Initial Tests	% DC Zero Shifts*/Testing Date/# Shocks
Endevco 2264A-50K (AA64)	6/74	0.45/3-75†	0.2/4-75†/~100 0.04/5-75†/~200
PCB 305A (441)	6/74	0.9/3-75†	0.4/4-75†/~100 0.1/4-76†/~200
PCB 305A02 (356)	7/73	1.0/3-75†	0.3/4-75†/~100 0.05/5-75†/~200 0.05/4-76†/~400
Endevco 2264A-50K (AB50)	6/74	Used on ESSEX	0.2/4-76†/~100
Endevco 2264A-10K (AD48)	9/75	0.02±0.02/3-76	0.005/4-76†/~200
Endevco 2264A-5K (AC74)	11/75	0.2±0.2/4-76	0.04/4-76†/~200

*If the shift was directly observed in the acceleration signal, it was calculated as

$$\% \text{ Shift} = \frac{[(\text{Acc. Signal After Shock}) - (\text{Acc. Signal Pre-Shock})]}{(\text{Peak Acceleration Signal})} * 100$$

†Shifts not directly observed were calculated from the velocity signal as

$$\% \text{ Shift} = \frac{[(\text{Slope of Vel. Signal Post Shock}) - (\text{Slope of Vel. Signal Pre-Shock})]}{(\text{Peak Acceleration Signal})} * 100$$

entry in the table is the average of the absolute value of the shifts and that we also quote the standard deviation of the mean for some of the tests.

Our facilities won't allow us to test the original units at their peak ratings. However, we did purchase two new transducers with ratings closer to our laboratory's capabilities. At receipt, both units had fairly small hysteresis characteristics. For the accelerometer rated at 10^5 m/sec^2, the average zero shift is buried in the digitizing noise (one part in 4096 is 0.024 percent). The zero shift of the other accelerometer (rated at 5×10^4 m/sec^2) is 0.04 percent.

The last transducer tested was recovered from a velocity gauge fielded on the ESSEX 1974 test series. While an apparent electronic or cable failure prevented us from recording the accelerometer's response to the ESSEX event, data from other nearby gauges imply that this accelerometer expeienced a shock well over 10^5 m/sec^2. Its zero shift in our laboratory tests is characteristic of a partially aged unit.

While we have not fully explored the second question, it does appear that the aging is not strongly dependent on the ratio of test level to peak rating. More extensive facilities and a much larger sample of accelerometers would need to be tested to answer the question. A definitive solution may not be possible because the "art" of transducer manufacture is continually changing. For example, one company (Endevco) has informed us that changes in internal construction, epoxies, delicate connecting wires, etc. have been and will be made at any time without corresponding model number changes. These might very easily affect subtle effects like zero shift. Perhaps our most recently purchased units show improved performance because of such internal modifications. Under these circumstances, we recommend that a transducer user keep in mind the potential deleterious effects of zero shift. If the quantity of interest is the integral of the

transducer's output and long measuring times are desired, the user should define an acceptable level of zero shift for his application (e.g., 1 percent or 0.1 percent, etc.) and then screen the actual purchased units for this effect.

With respect to the last question, in our recent tests changes in the average dc shift have not been observed; all of our units seem "well-aged." Thus no improvements in the ac shift were observed. However, amongst the five accelerometers, there does seem to be a monotonic relation between the two types of shift; see Table 6. Note that we give the ac shift as the magnitude of velocity at the shock beginning, extrapolated back from the post shock velocity signal. If we associate this shift with the risetime of the shock, about 500 μs, then one m/sec represents 2000 m/sec^2 or 10 percent of the peak acceleration. It appears that the ac shift can be quite significant* and that if the dc shift is small, the ac shift is also reduced in importance.

---

*The peak velocities of the accelerometers in these tests were about ± 2 to 3 m/sec.

Table 6. Comparison of ac and dc Zero Shifts.*

Accelerometer	Endevco 2264A-10K	Endevco 2264A-5K	PCB 305A02	PCB 305A	Endevco 2264A-50K
Mean DC Shift (%)	0.005 ±0.003	0.04 ±0.07	0.05 ±0.04	0.11 ±0.09	0.18 ±0.17
Mean AC Shift (m/s)	0.028 ±0.025	0.13 ±0.09	0.34 ±0.31	0.50 ±0.39	1.1 ±0.8

*Test Environment: Peak Acceleration ±2 x 10^4 m/sec^2; Peak Velocity 3 m/sec; Risetime 500 μs; Duration ~50 ms; Net Displacement 0.0 cm.

SECTION VI

FIELD CALIBRATION OF GROUND MOTION INSTRUMENTS

The original work planned under this contract called for S^3 to devise methods for mechanical calibration of stress and motion gauge systems in the field. However, the actual need for a calibration per se of stress and velocity gauges in the field is not clear. It is standard procedure at S^3 (and probably at other DNA contractors) for all gauges to be calibrated subsequent to their manufacture by or delivery to the contractor and prior to shipment of the gauges to a test site. If there are any doubts about the calibrations, the doubts are resolved at the contractor's home facility and not in the field where working conditions are inferior.

However, it is often desirable to determine if the gauges (and their preamplifiers, if appropriate) are functional following transit and if they are performing with approximately the same sensitivity they exhibited before shipment. In the case of gauges employed for free-field measurements in the earth, a check must necessarily be made before the gauges are installed in the ground because of their inaccessibility after their emplacement. For gauges used in accessible areas such as those mounted on structures which are to be grouted later, this functional test could be performed after gauge installation. In any event, the check needs to be done before the gauges are made irretrievable. To perform the field qualification, one would like to have a portable device that could generate a stress or velocity (as appropriate) of reproducible (to ± 10 or 20 percent) magnitude. In this way, moderate aberrations in gauge performance could be detected. The signal generated by the gauge in the field would be observed and compared with the signal generated by the gauge when tested before shipment. This preshipment test would best be performed at the time of

gauge calibration to assure that the signal generated is valid. Once such a reference signal is established, the functioning of the gauge can be tested at any time by use of the testing apparatus.

The unit can be relatively simple, employing the impact of a spring-loaded mass to generate the stresses and motions. Spring loaded devices can be made reasonably reproducible and reliable. For example, in order to test the S^3 quartz stress gauge, the instrument could be clamped to a base assembly; a rod of some moderate length, say two feet, would impact the gauge piston and be allowed to rebound. If the rod is propelled at a reproducible velocity, the impulse delivered to the transducer should be reproducible. This concept is essentially the same one presently used in calibrating our stress gauges. In order to test a velocity gauge, the instrument would be located perhaps 10 centimeters off the base on an easily collapsible mount. During the millisecond bar-instrument impact, the gauge would be in "free flight" and its signal could be compared with that predicted by conservation of momentum. The design of such test devices should require only a small effort. Somewhat different designs would probably be necessary for different gauge types.

REFERENCES

Batt, R. G., (March 1975), "PRE-MINE THROW IV, Free Field Thermal Measurements," TRW Inc., POR 6831.

Behrens, W., (1971), "Total Temperature Thermocouple Probe Based on Recovery Temperature of Circular Cylinder," Int. J. Heat and Mass Transfer, 14, p. 1621.

Boyer, D. W. and R. C. Parkhurst, (1971), Pressure-Probe Methods for Determining Wind Speed and Flow Direction, Her Majesty's Stationary Office, London.

Cady, W. G., (1964), Piezoelectricity, Volume 1, p. 77, Dover Publications, New York.

Coleman, P. L., W. G. Ginn and D. R. Grine, (September 1975), "Ground Motion Gauge Development," Systems, Science and Software, Defense Nuclear Agency Report DNA POR 3702F.

DeCarli, P. S., (June 1974), "Stress Gage System for the Megabar Range,: Defense Nuclear Agency Report DNA 3593F.

Flanders, P. L., (Ed.), (May 1964), Nuclear Geoplosics, Volume III, Defense Nuclear Agency Report DNA 1285.

Gaffney, E. S., H. R. Kratz and J. R. Barthel, (1976), "Suggested Measurements for HURON KING," Systems, Science and Software Topical Report SSS-R-76-2889.

Ginsberg, M. J., (1973), "Effects of Stress on the Electrical Resistance of Ytterbium and Calibration of Ytterbium Stress Transducers," Stanford Research Institute, Defense Nuclear Agency Report DNA 3577F.

Glenn, H. D., (October 1973), "Development of Diagnostic Techniques for Application to Underground Nuclear Tests," Defense Nuclear Agency Report DNA 3257F.

Graham, R. A. and R. D. Jacobson, (1973), "Lithium Niobate Stress Gauge for Pulsed Radiation Deposition Studies," Appl. Phys. Ltr. 23, 584.

Graham, R. A., (August 1974), "Linear and Nonlinear Piezoelectric Constants of Quartz, Lithium Niobate and Lithium Tantalate," in Proceedings, Microwave Acoustics Symposium, University of Lancaster.

Grine, D. R. and P. L. Coleman, (June 1974), "Ground Motion Gauge Development," Systems, Science and Software, Defense Nuclear Agency Report DNA 3524T.

Grine, D. R., (October 1975), "Hardened Quartz Gauges for Ground Shock and Airblast Measurements," paper presented at Defense Nuclear Agency Ground Motion and Blast Instrumentation Conference, Vicksburg, Mississippi.

Horning, R. R. and W. M. Isbell, (1975), "Calibration Studies of the Carbon Piezoresistive Gauge," Rev. Sci. Instr., 46, p. 1374.

Keough, D. D., (March 1970), "Development of a High-Sensitivity Piezoresistive Shock Transducer for the Low Kilobar Range," Stanford Research Institute Final Report DASA-69-C-0014.

Keough, D. D., (1974), unpublished.

Knasel, T. M., (1975), "Solar Furnace Experiments," Science Applications, Inc. (notes dated August 27, 1975).

Kovarsznay, L. S. G., (1954), "Hot Wire Method," Physical Measurements in Gas Dynamics and Combustion, Princeton University Press, Princeton, New Jersey.

Kratz, H. R. and R. E. Rinehart, (April 1974), "DIAMOND MINE Event, Diagnostic Measurements," Systems, Science and Software, Defense Nuclear Agency Report POR 6572.

Kratz, H. R., (May 1975), "HYBLA FAIR Event, Diagnostic Measurements," (Draft) Systems, Science and Software Project Officer's Report SSS-R-75-2631.

Liepmann, H. W. and Roshko, A., (1957), Elements of Gas Dynamics, John Wiley and Sons, Inc., New York.

Marble, F. E., (1970), "Dynamics of Dusty Gases," Ann. Rev. Fluid Mech., 2, Palo Alto.

Moore, E. T., Jr., D. M. Mumma, D. R. Randall, C. S. Godfrey, and T. W. Lee, (May 1975), "BOSS Design Validation," Physics International Company, Defense Nuclear Agency Report DNA 3622F.

Nauman, W. J., (1975), unpublished.

Petersen, C. F., (February 1973), "Fielding of Ytterbium Stress Transducers on DIAMOND MINE and DIAGONAL LINE, Final Report Task II," Defense Nuclear Agency Report DNA 3086F.

Petersen, C. F., (April 1975), "Stress and Particle Velocity Measurements on 1000-lb Shots in Porous Rocks," (Draft) Stanford Research Institute Project PYU-3698, Contract No. DNA001-75-C-0077.

Reed, R. P., (March 1975), "Lithium Niobate Free-Field Stress Measuring System for the Rock Springs, Wyoming, Oil Shale In Situ Retorting Experiment of the U. S. Bureau of Mines," Sandia Laboratories, SAND74-0396.

Rice, M. H., (May 1976), Systems, Science and Software, private communication.

Rowland, R. H., (August 1967), "Blast and Shock Measurement State-of-the-Art Review," DASIAC Special Report 45.

Smith, C. W., (1971), "Dynamic Measurements of Stress Pulses in Tuff at Nevada Test Site," Stanford Research Institute, Defense Nuclear Agency Report DNA 2811F; corrected waveforms based on revised calibration data are presented by A. H. Jones, and S. J. Green, (1973), "The Role of Material Properties in Determining Ground Motion from High Energy Detonators," Terra Tek, Inc., Defense Nuclear Agency Report DNA 3056F.

Smith, C. W., (November 1973), "Ytterbium Gage Measurements in DIDO QUEEN and HUSKY ACE," Final Report, Stanford Research Institute, prepared for Systems, Science and Software. Measurements also reported by R. E. Rinehart in Defense Nuclear Agency Reports POR 6785, February 1974 and POR 6809, April 1974, both by Systems, Science and Software.

Suits, C. G. and H. Poritsky, (1935), "Determination of Arc Temperature from Sound Velocity Measurements," Physics, Volume 6, p. 190-202.

Vortman, L. J. and J. A. Beyeler, (November 1974), "Results of Ground Motion and Airblast Measurements, Project ESSEX I, Phase I," Sandia Laboratories, SLA-73-0918.

APPENDIX A

RAW DATA RECORDS FOR HARDPAN I-2B

(1000 psi = 69 bar = 2.9 x 10^6Pa)

AD-A035 710 SYSTEMS SCIENCE AND SOFTWARE LA JOLLA CALIF F/G 14/2
REVIEW AND DEVELOPMENT OF GROUND MOTION AND AIRBLAST INSTRUMENT--ETC(U)
JUN 76 P L COLEMAN, E S GAFFNEY, W G GINN DNA001-75-C-0008
UNCLASSIFIED SSS-R-76-2945 DNA-4036F NL

2 OF 2
AD A035710

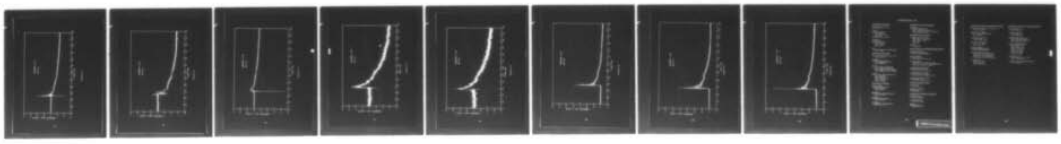

END
DATE FILMED
3-77

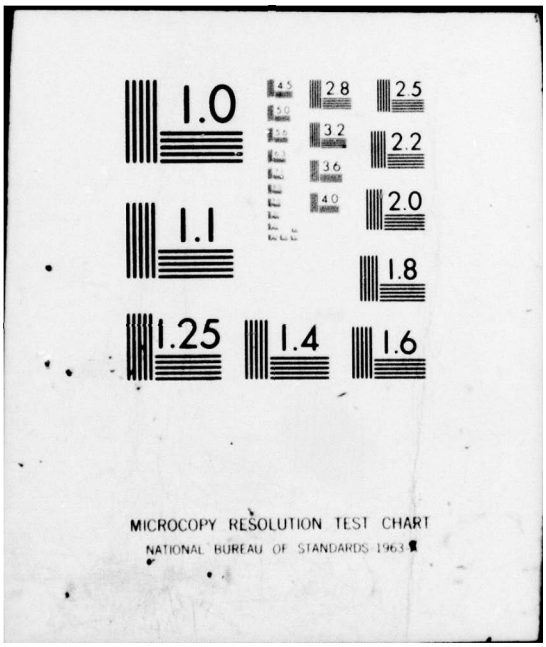
1.0
1.1
1.25
1.4
1.6
1.8
2.0
2.2
2.5
2.8
3.2
3.6
4.0
MICROCOPY RESOLUTION TEST CHART
NATIONAL BUREAU OF STANDARDS-1963-A

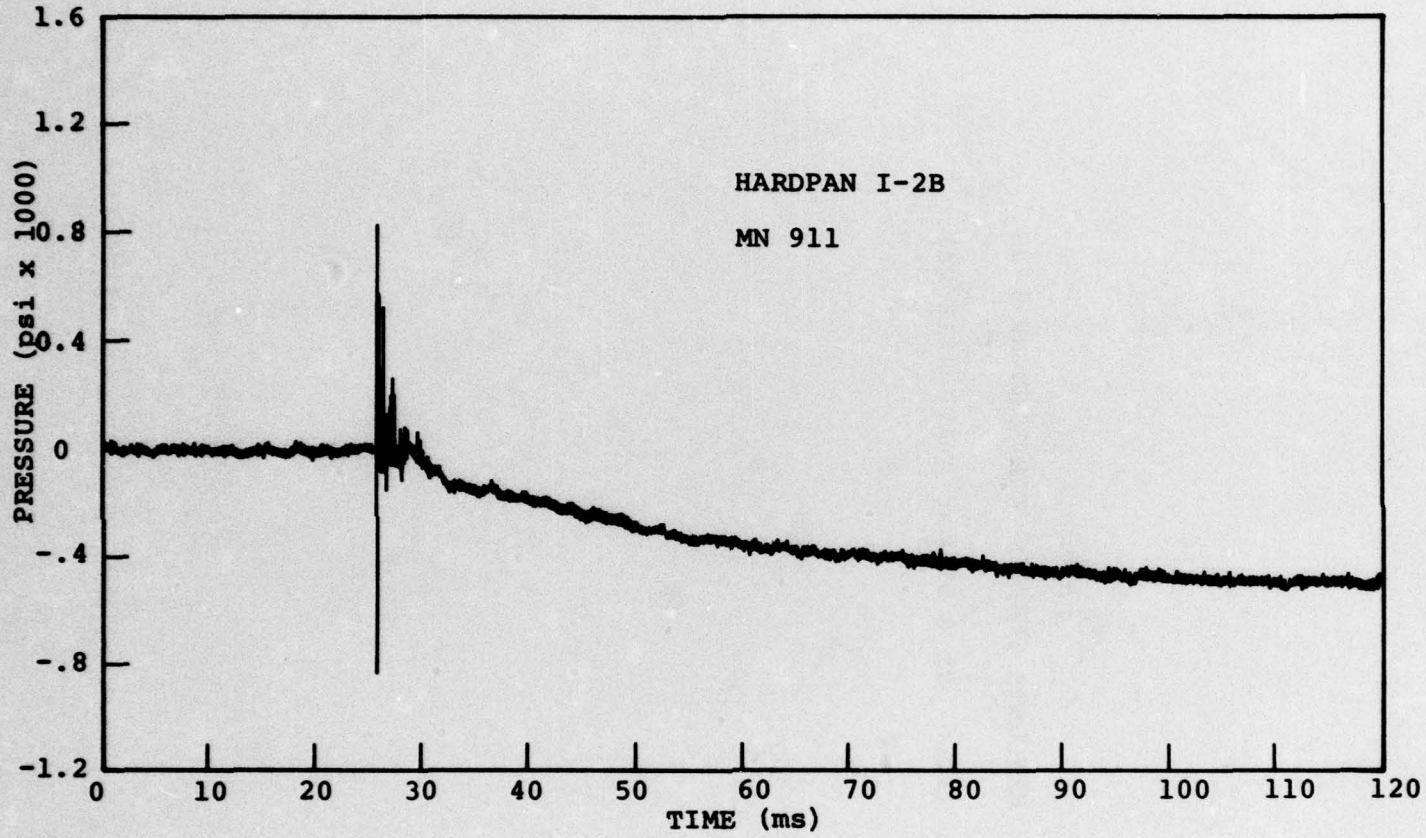
HARDPAN I-2B
MN 911
PRESSURE (psi x 1000)
1.6
1.2
0.8
0.4
0
-.4
-.8
-1.2
0
10
20
30
40
50
60
70
80
90
100
110
120
TIME (ms)

Figure A1.

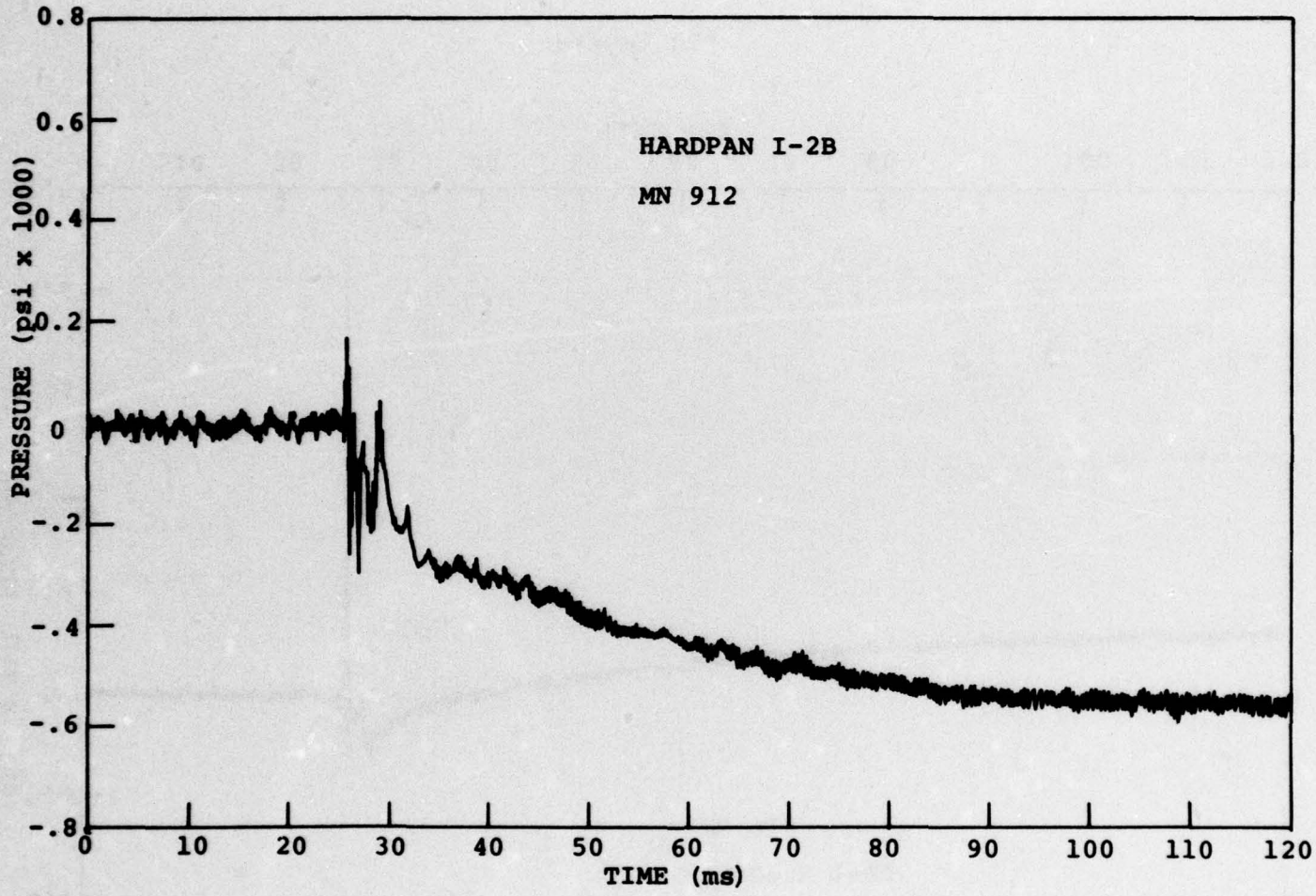
HARDPAN I-2B
MN 912
PRESSURE (psi x 1000)
0.8
0.6
0.4
0.2
0
-.2
-.4
-.6
-.8
0
10
20
30
40
50
60
70
80
90
100
110
120
TIME (ms)

Figure A2.

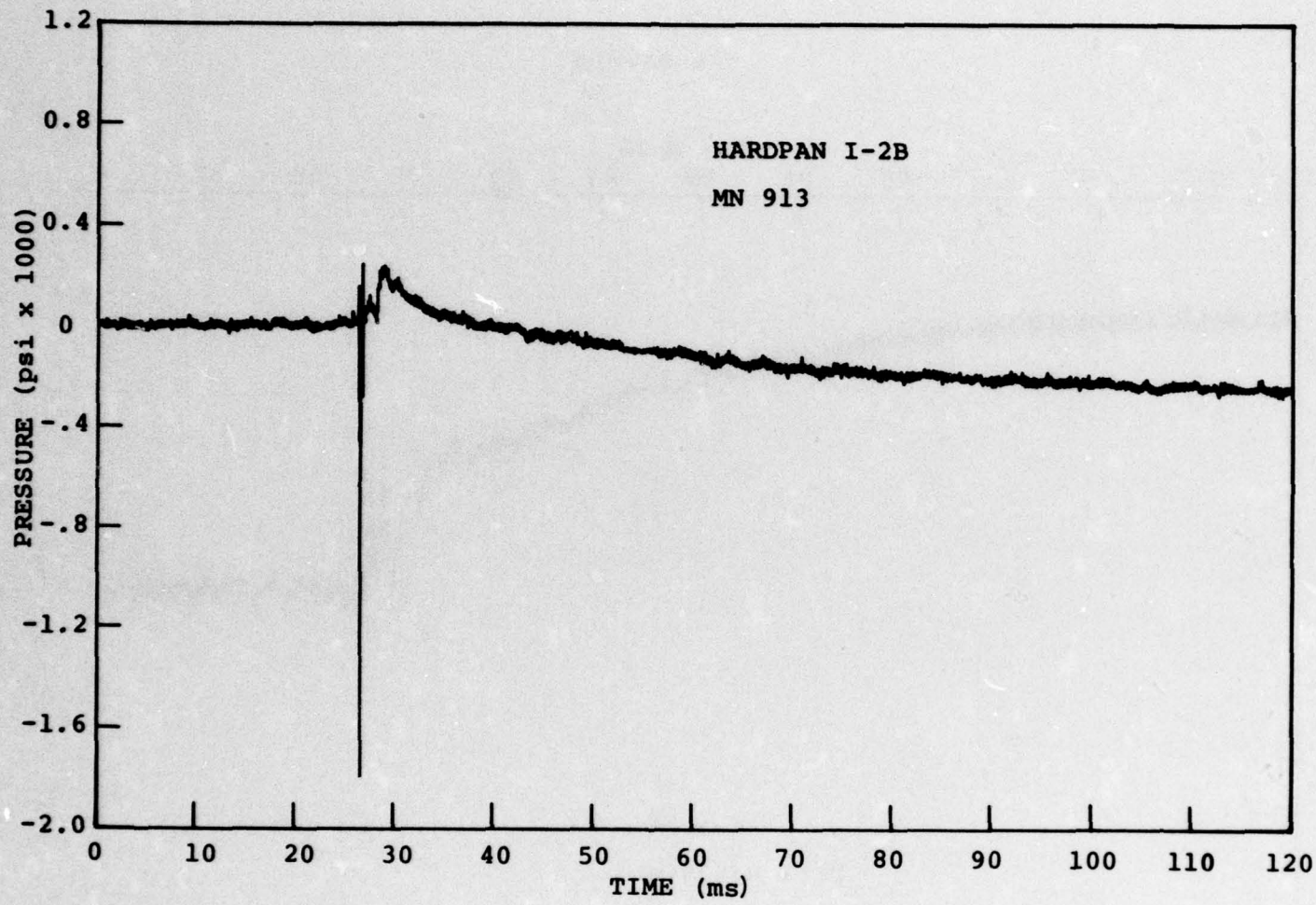
HARDPAN I-2B
MN 913
PRESSURE (psi x 1000)
1.2
0.8
0.4
0
-.4
-.8
-1.2
-1.6
-2.0
0
10
20
30
40
50
60
70
80
90
100
110
120
TIME (ms)

Figure A3.

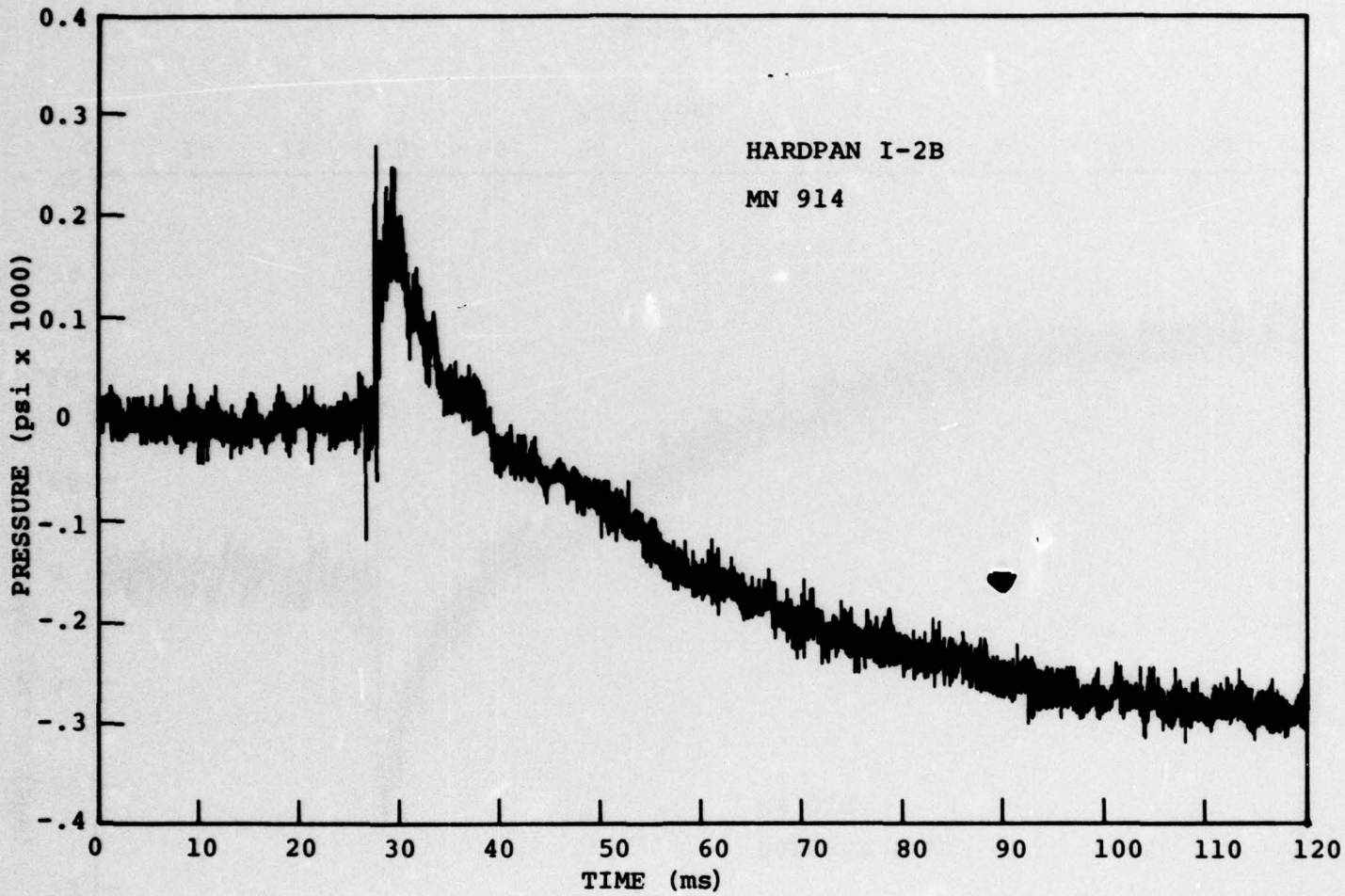
HARDPAN I-2B
MN 914
PRESSURE (psi x 1000)
0.4
0.3
0.2
0.1
0
-.1
-.2
-.3
-.4
0
10
20
30
40
50
60
70
80
90
100
110
120
TIME (ms)

Figure A4.

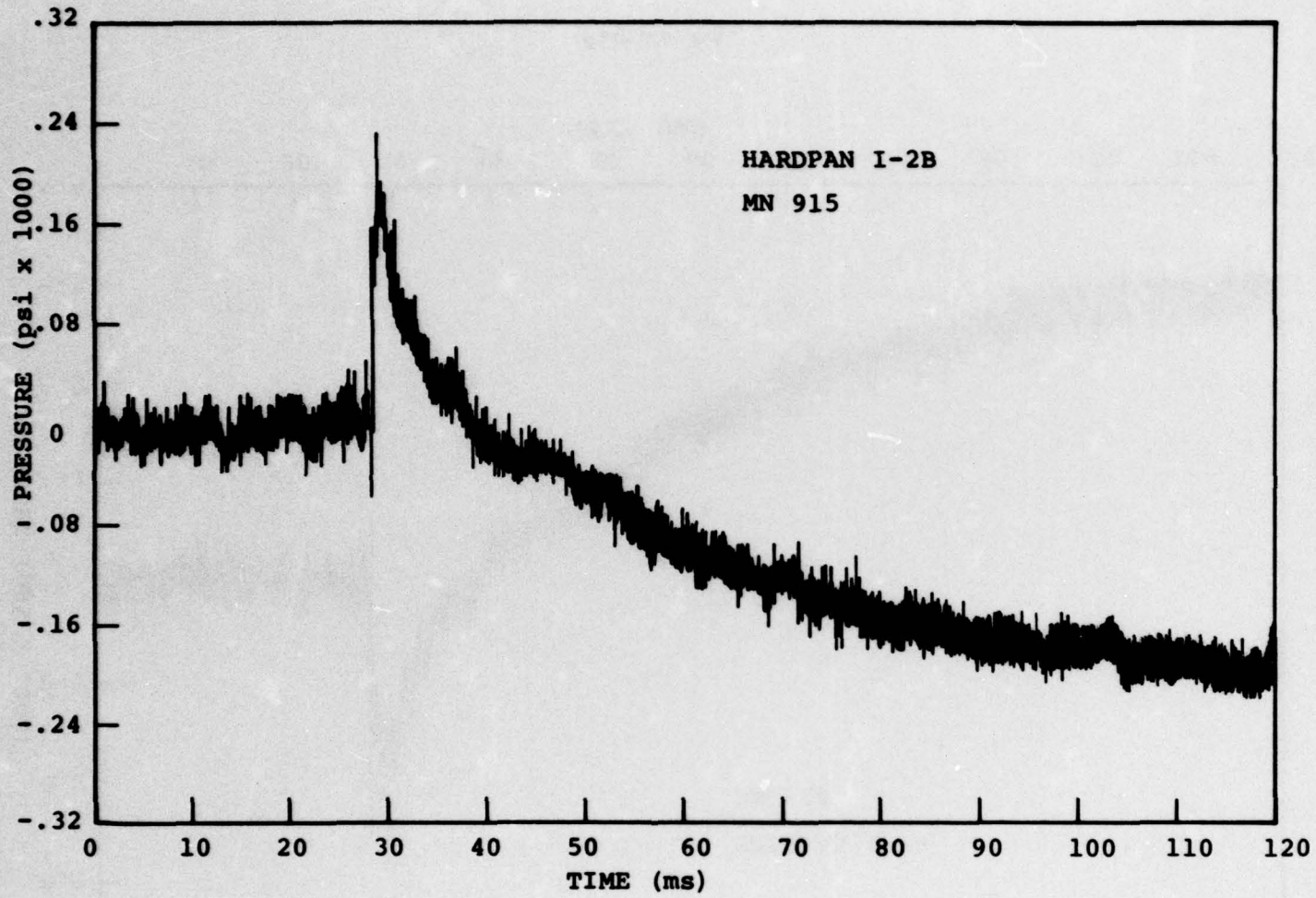
HARDPAN I-2B
MN 915
PRESSURE (psi x 1000)
.32
.24
.16
.08
0
-.08
-.16
-.24
-.32
0
10
20
30
40
50
60
70
80
90
100
110
120
TIME (ms)

Figure A5.

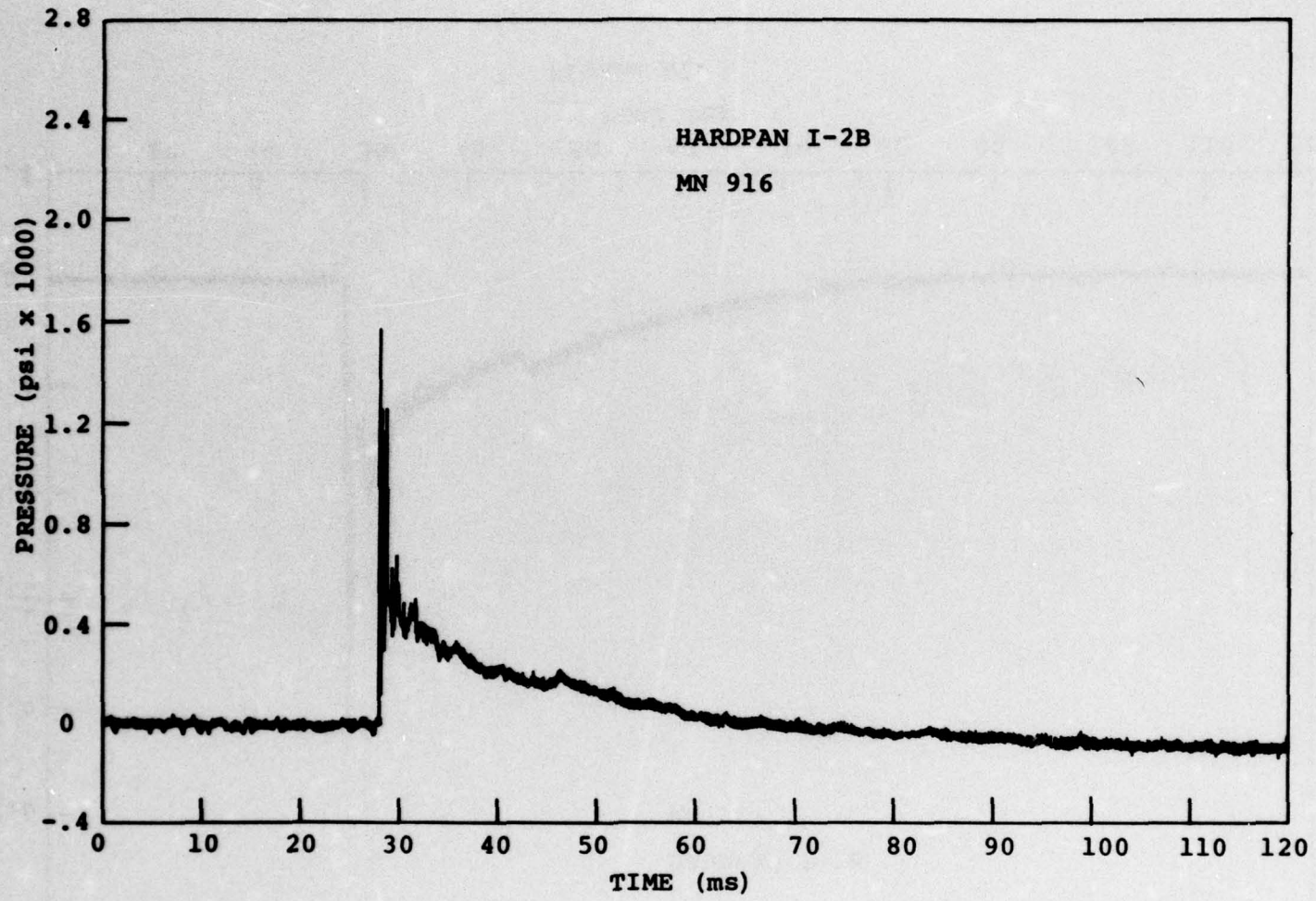
HARDPAN I-2B
MN 916
PRESSURE (psi x 1000)
2.8
2.4
2.0
1.6
1.2
0.8
0.4
0
-.4
0
10
20
30
40
50
60
70
80
90
100
110
120
TIME (ms)

Figure A6.

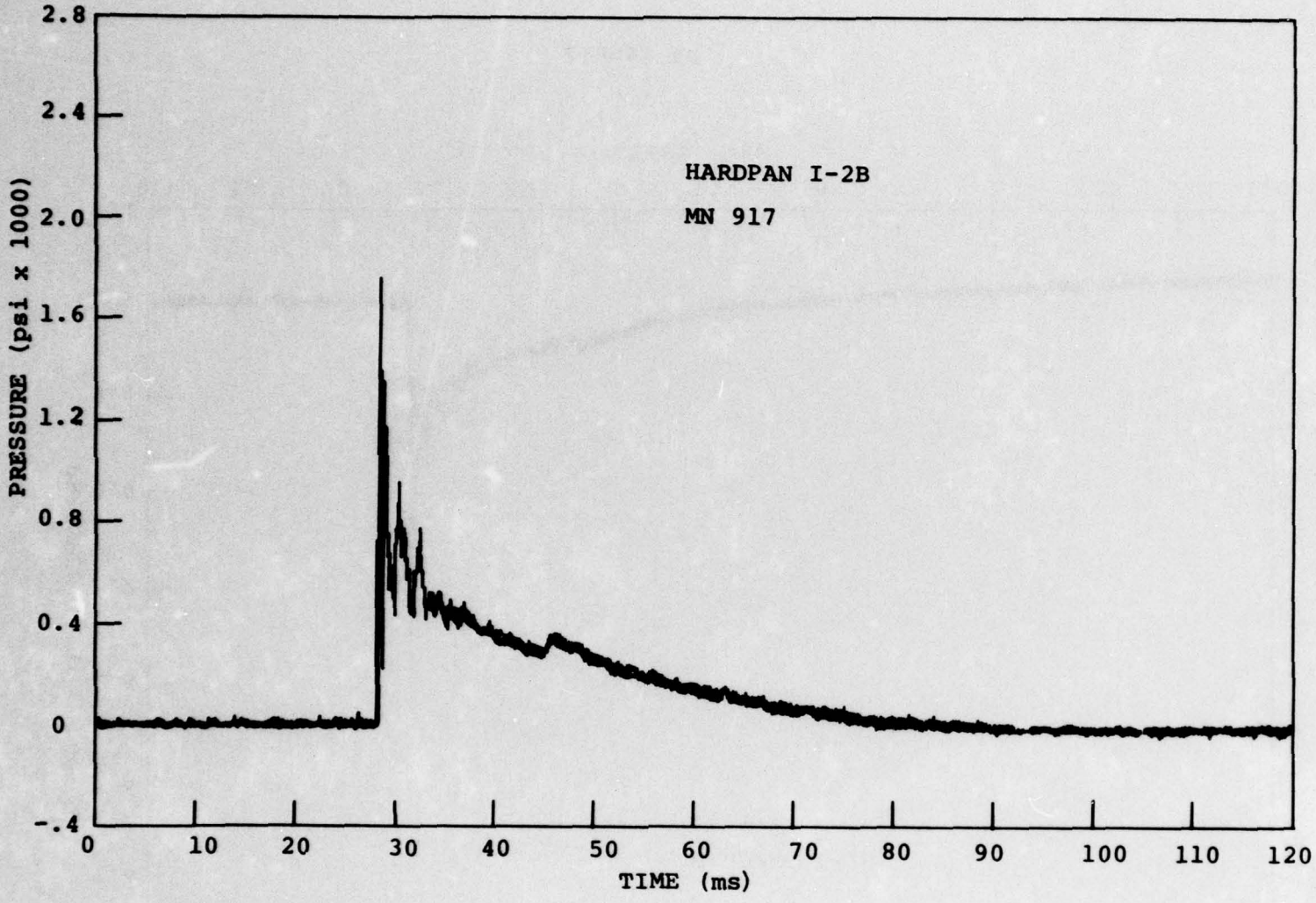
HARDPAN I-2B
MN 917
PRESSURE (psi x 1000)
2.8
2.4
2.0
1.6
1.2
0.8
0.4
0
-.4
0
10
20
30
40
50
60
70
80
90
100
110
120
TIME (ms)

Figure A7.

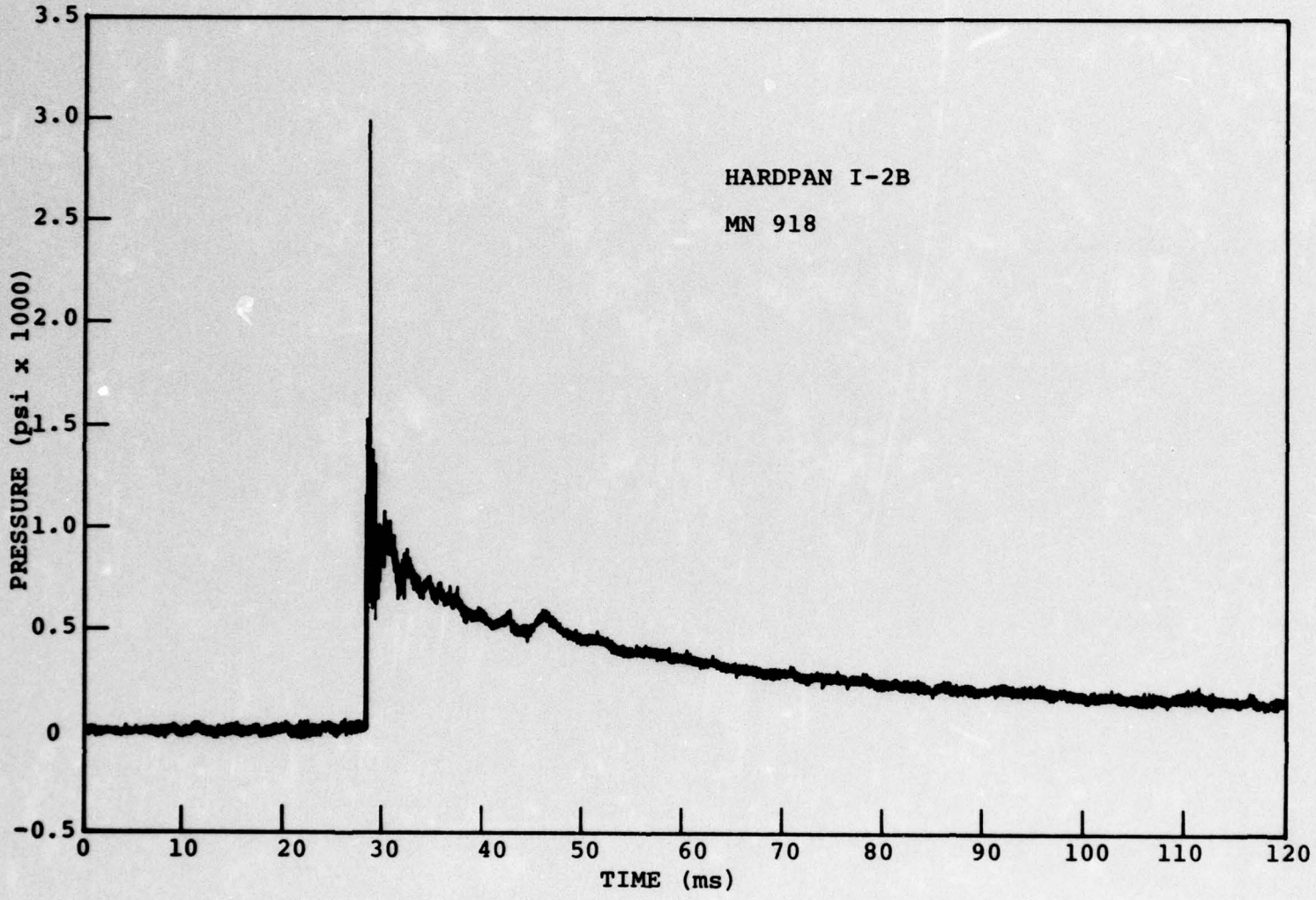
HARDPAN I-2B
MN 918
PRESSURE (psi x 1000)
3.5
3.0
2.5
2.0
1.5
1.0
0.5
0
-0.5
0
10
20
30
40
50
60
70
80
90
100
110
120
TIME (ms)

Figure A8.

DISTRIBUTION LIST

DEPARTMENT OF DEFENSE

Defense Documentation Center
12 cy ATTN: TC

Director
Defense Nuclear Agency
ATTN: DDST
ATTN: STSI, Archives
2 cy ATTN: SPSS
3 cy ATTN: STTL, Tech. Lib.

Commander
Field Command
Defense Nuclear Agency
ATTN: FCPR
ATTN: FCTMOF
ATTN: FCT

Chief
Livermore Division, Fld. Command, DNA
ATTN: FCPRL

DEPARTMENT OF THE ARMY

Dep. Chief of Staff for Rsch., Dev. & Acq.
ATTN: Tech. Lib.

Commander
Harry Diamond Laboratories
ATTN: DRXDO-TI, Tech. Lib.
ATTN: DRXDO-NP

Director
U.S. Army Ballistic Research Labs.
ATTN: Tech. Lib., Edward Baicy
ATTN: DRXBR-TL-IR, J. H. Keefer
ATTN: DRXBR-X, Julius J. Meszaros

Director
U.S. Army Engr. Waterways Exper. Sta.
ATTN: Leo Ingram
ATTN: Tech. Lib.
ATTN: William Flathau
ATTN: F. Hanes
ATTN: A. Peckna

DEPARTMENT OF THE NAVY

Officer-in-Charge
Civil Engineering Laboratory
ATTN: Tech. Lib.
ATTN: W. Shaw

Commander
Naval Facilities Engineering Command
ATTN: Tech. Lib.

Commander
Naval Ship Engineering Center
ATTN: Tech. Lib.

Commander
Naval Ship Rsch. & Development Ctr.
ATTN: Tech. Lib.

DEPARTMENT OF THE NAVY (Continued)

Commander
Naval Surface Weapons Center
ATTN: Code WX-21, Tech. Lib.
ATTN: Code WA-501, Navy Nuc. Prgms. Off.
ATTN: Code 241, J. Petes

DEPARTMENT OF THE AIR FORCE

AF Weapons Laboratory, AFSC
ATTN: DES, M. A. Plamondon
ATTN: DEX, J. Renick
ATTN: SUL
ATTN: DEX

HQ USAF/IN
ATTN: INATA

ENERGY RESEARCH & DEVELOPMENT ADMINISTRATION

University of California
Lawrence Livermore Laboratory
ATTN: Tech. Info., Dept. L-3

Sandia Laboratories
Livermore Laboratory
ATTN: Doc. Con. for Tech. Lib.

Sandia Laboratories
ATTN: Doc. Con. for Luke J. Vortman
ATTN: Doc. Con. for Org. 3422-1, Sandia Rpt. Coll.
ATTN: Doc. Con. for A. J. Chabai

U.S. Energy Rsch. & Dev. Admin.
Albuquerque Operations Office
ATTN: Doc. Con. for Tech. Lib.

U.S. Energy Rsch. & Dev. Admin.
Division of Headquarters Services
ATTN: Doc. Con. for Class. Tech. Lib.

U.S. Energy Rsch. & Dev. Admin.
Nevada Operations Office
ATTN: Doc. Con. for Tech. Lib.

OTHER GOVERNMENT AGENCIES

Bureau of Mines
ATTN: Tech. Lib.

Department of the Interior
Bureau of Mines
ATTN: Tech. Lib.

DEPARTMENT OF DEFENSE CONTRACTORS

Agbabian Associates
ATTN: M. Agbabian

Artec Associates, Inc.
ATTN: D. W. Baum

EG&G, Inc.
Albuquerque Division
ATTN: Tech. Lib.

DEPARTMENT OF DEFENSE CONTRACTORS (Continued)

Electromechanical Systems of New Mexico, Inc.
ATTN: R. A. Shunk

General Electric Company
TEMPO-Center for Advanced Studies
ATTN: DASIAC

Kaman Sciences Corporation
ATTN: Library
ATTN: Donald C. Sachs

Merritt Cases, Incorporated
ATTN: J. L. Merritt
ATTN: Tech. Lib.

Nathan M. Newmark
Consulting Engineering Services
ATTN: Nathan M. Newmark

Physics International Company
ATTN: Doc. Con. for Fred M. Sauer
ATTN: Doc. Con. for Tech. Lib.
ATTN: Doc. Con. for James Shea
ATTN: Doc. Con. for Charles Godfrey

R & D Associates
ATTN: J. G. Lewis
ATTN: Tech. Lib.
ATTN: Henry Cooper

DEPARTMENT OF DEFENSE CONTRACTORS (Continued)

Science Applications, Inc.
ATTN: Tech. Lib.

Terra Tek, Incorporated
ATTN: Tech. Lib.
ATTN: Sidney Green

Stanford Research Institute
ATTN: George R. Abrahamson
ATTN: SRI, Library, Rm. G-021
ATTN: Douglas D. Keough

Systems, Science & Software, Inc.
ATTN: Donald R. Grine
ATTN: Tech. Lib.
ATTN: Robert T. Allen
ATTN: P. L. Coleman
ATTN: Carl Petersen
ATTN: E. S. Gaffney
ATTN: W. G. Ginn
ATTN: H. R. Kratz

TRW Systems Group
ATTN: Tech. Info. Ctr., S-1930
ATTN: Paul Lieberman

The Eric H. Wang Civil Engineering Rsch. Fac.
ATTN: Neal Baum